

Article

# Flash Flood Hazard Assessment along the Red Sea Coast Using Remote Sensing and GIS Techniques

Mohamed Rashwan <sup>1,2</sup>, Adel K. Mohamed <sup>1,3</sup>, Fahad Alshehri <sup>2,\*</sup>, Sattam Almadani <sup>2</sup>, Mohammed Khattab <sup>4</sup> and Lamees Mohamed <sup>1</sup>

<sup>1</sup> Geology Department, Faculty of Science, Mansoura University, Mansoura 11421, Egypt

<sup>2</sup> Abdullah Alrushaid Chair for Earth Science Remote Sensing Research, Geology and Geophysics Department, College of Science, King Saud University, Riyadh 11451, Saudi Arabia

<sup>3</sup> Faculty of Basic Sciences, New Mansoura University, New Mansoura 35712, Egypt

<sup>4</sup> Department of Geography, Faculty of Arts, Cairo University, Giza 11321, Egypt

\* Correspondence: falshehria@ksu.edu.sa; Tel.: +966-114677053

**Abstract:** The Egyptian Red Sea coast is periodically exposed to flash floods that cause severe human and economic losses. That is due to its hydro-geomorphological characteristics. Therefore, identifying flash flood hazards in these areas is critically important. This research uses an integrated approach of remote sensing data and GIS techniques to assess flash flood hazards based on morphometric measurements. There are 12 drainage basins in the study area. These basins differ in their morphometric characteristics, and their main streams range between the 4th and 7th order. The morphometric parameter analysis indicates that three wadis are highly prone to flooding, five wadis are classified as moderate hazard, and four wadis are rated under low probability of flooding. The study area has a probability of flooding, which could cause serious environmental hazards. To protect the region from flash flood hazards and the great benefit of rainwater, the study recommended detention, crossing, diversion, and/or storage of the accumulated rainwater by building a number of dams or culverts along the main streams of wadis to minimize the flooding flow.

**Keywords:** flood verification; hydro-morphometric analysis; flood hazard; GIS



**Citation:** Rashwan, M.; Mohamed, A.K.; Alshehri, F.; Almadani, S.; Khattab, M.; Mohamed, L. Flash Flood Hazard Assessment along the Red Sea Coast Using Remote Sensing and GIS Techniques. *ISPRS Int. J. Geo-Inf.* **2023**, *12*, 465. <https://doi.org/10.3390/ijgi12110465>

Academic Editor: Wolfgang Kainz

Received: 25 July 2023

Revised: 22 October 2023

Accepted: 7 November 2023

Published: 16 November 2023



**Copyright:** © 2023 by the authors. Licensee MDPI, Basel, Switzerland. This article is an open access article distributed under the terms and conditions of the Creative Commons Attribution (CC BY) license (<https://creativecommons.org/licenses/by/4.0/>).

## 1. Introduction

Flood hazard assessment is a vital issue in making appropriate strategies for development and planning in urban and desert regions, especially under the noticeable impacts of climate change as well as complex land use/land cover changes [1,2]. Flash flood is one of the natural disasters that affects the socio-economic and environmental aspects worldwide. It stands out among other natural disasters because they are more severe, cause damage to life, property, and infrastructure, and result in higher economic losses globally [3,4]. Flooding events are said to be responsible for nearly 44% of natural disaster deaths worldwide, particularly in arid regions [5]. According to Murray and Ebi [6], heavy rains that fall in a short time cause flash floods. Conversely, floods are a significant supply of water in desert wadis, particularly for recharging groundwater [7]. In this context, Egypt is heading towards the implementation of many projects quickly with the aim of creating economic growth capable of facing challenges and providing jobs, housing, and investment opportunities [7]. Egyptian Red Sea coast development is among the most significant future visions that the government takes into consideration. Therefore, it has great strategic importance for tourism, mining, and building materials [8]. Flash floods continue to recharge Egypt's groundwater reservoirs, particularly along the Red Sea [9], which were recharged throughout the earlier rainy periods like Pluvial times [10]. Therefore, good planning of any long-term development project requires the study of flash flooding for risk assessment and flood mitigation [11].

The current study provides an integrated approach of geographic information system (GIS) technique and remotely sensed (RS) satellite data images for the objectives of hydromorphometric analysis and flash flood hazards assessment. The GIS can help to determine the basin boundary and stream networks from remote sensing-derived digital elevation models (DEMs), drive the morphometric parameters, and assess flash flood hazards. The morphometric measurements of the catchments, such as linear, areal, and relief, are closely related to flash flood susceptibility [12]. Morphometry is the numerical analysis of the different watershed characteristics, including area, stream number and order, total stream length, basin length, width, perimeter, shape factor, stream density, stream frequency, drainage basin texture, ruggedness number, and basin slope. The morphometric measurements provide useful information for geological, hydrological, and flash flood susceptibility modeling [13].

In several studies, flash floods have been evaluated using RS and GIS. (e.g., [14–16]). In Abd El Aal et al. study [14], the ranking method and the El Shamy approach were used separately to assess flood hazard. Elsadek et al. [15] used the multi-method technique to assess and monitor flood mitigation and planning processes, using the El Shamy approach and the ranking method. Nasir et al. [16] matched the El Shamy approach and ranking method in order to estimate flood hazards. Only linear and areal morphometric parameters were used in the last study to construct the ranking method. These approaches are the two most important geospatial methods for assessing the probability of flash floods using morphometric parameters [16]. Additionally, these studies built on investigating a single large basin containing a number of sub-basins.

The current study focused on studying the flood risks of a group of basins that cross the area located on the Red Sea coast to protect roads and facilities. The primary objectives of the current study are the integration and matching between two approaches (El Shamy's approach and ordinary ranking method) to extract at-risk basins. El Shamy's approach and ranking method were built using a sufficient number of hydro-morphometric measurements (linear, area, and relief). In light of this, an understanding of hydrologic processes is essential for the proper management of water resources in watersheds, especially in ungauged watersheds where hydrometeorological data are not available. In the absence of actual measured hydrologic data, numerical morphometric analysis can provide useful information on the watershed's geology and hydrologic features [17,18]. The flash flood assessment methods still have limitations, as the different parameters and methods used may lead to a different evaluation degree. So, it is important to validate the flash flood assessment. In this regard, due to the difficulty and lack of measurements of actual runoff hydrograph at the wadi outlet, the flash flood assessment was validated in the current study based on the field examination and historical flash floods obtained from satellite images.

## 2. Study Area

The study area is part of the Red Sea Governorate, Egypt, and extends along the Red Sea coast between latitudes  $25^{\circ}17'51.382''$  and  $25^{\circ}59'19.57''$  N and longitudes  $34^{\circ}0'7.682''$  and  $34^{\circ}38'32.543''$  E. It is located about 22 km south of QuseirCity and about 58 km north of MarsaAlamCity. It covers 2253 km<sup>2</sup>. It is easily reached through the Red Sea Coastal Road, which is bounded from the east side, or through MarsaAlam International Airport, located on the southern east side of the area (Figure 1).

From a meteorological point of view, the climate of the study area is typically hyper-arid, with hot, dry summer and cold to warm winter [19]. According to the Qu seir meteorological surface station, which is located at a distance of 20 km north of the study area. The mean day temperature ranges between 18.05 °C in January and 30.55 °C in August. The minimum day temperature is 7 °C in January, and the maximum day temperature is 43 °C in May [20]. The rain falls in small quantities in a day or in a few days in winter, and somewhere in spring and autumn, the mean annual is 6.42 mm. Very small amounts of rainfall with an annual average of 6.42 mm, and this rain is not responsible for the occurrence of flashfloods, but during tropical rainstorms, large amounts of rain may fall

within a few hours and sometimes up to a day or more. This rain is characterized by being spotty and sometimes covers hundreds of square kilometers, as was the case in the storms of October 2016 [21] and March 2020 [22]. These rains resulted in torrential flows, and the maximum amount of rain recorded in Qu seir station was 20, 15.2, and 13.8 mm on the dates of 18 October 1997, 30 January 1997, and 17 November 1996. This abnormal quantity of rain is responsible for flashfloods.

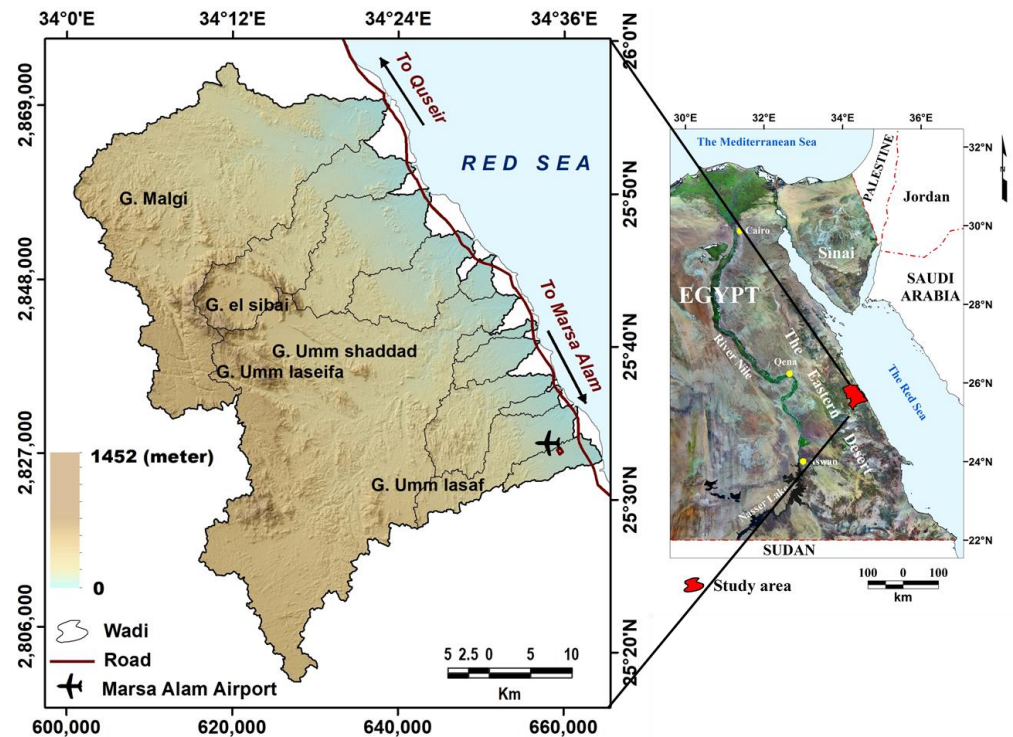
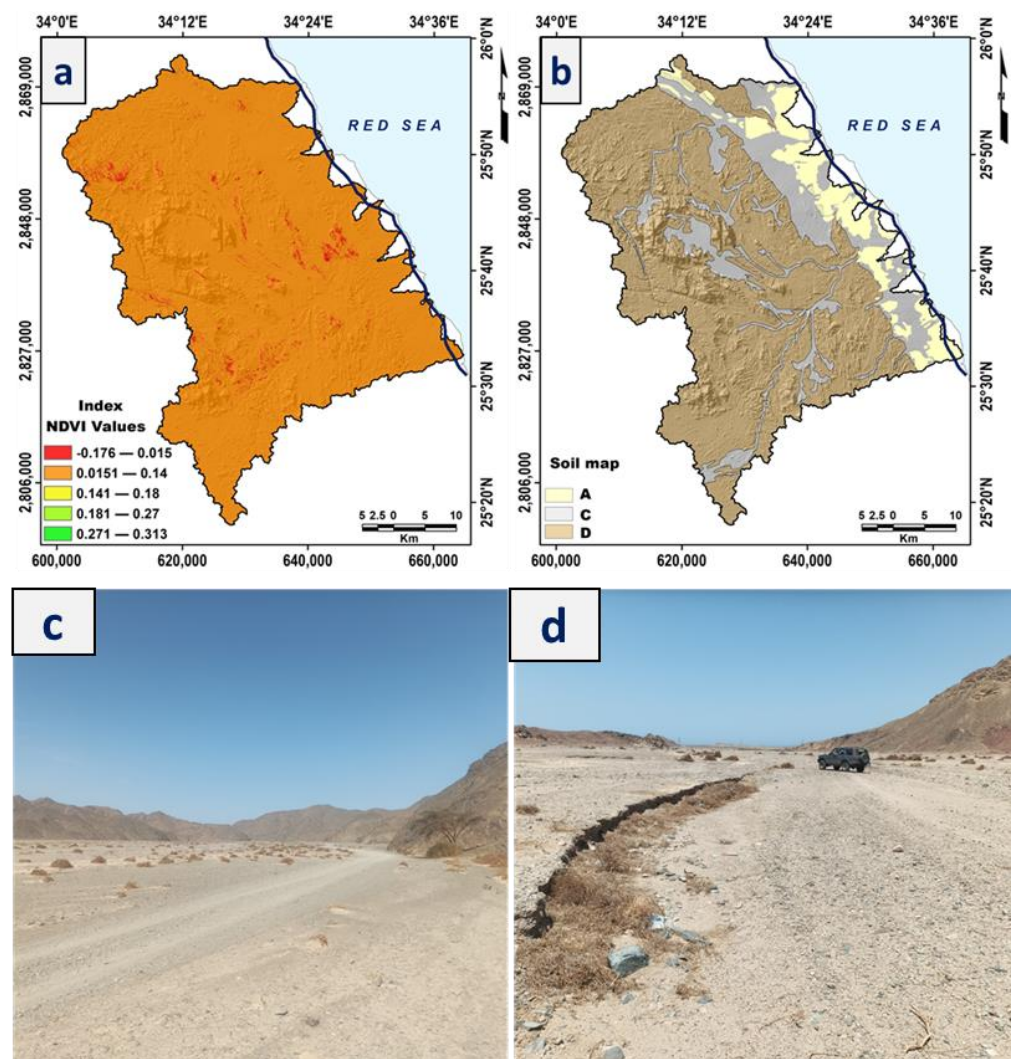


Figure 1. Location map of the study area.

Along with a meteorological description of the study area, the soil type and land cover must also be considered because they play a significant role in maximizing the flash flood impact. Although climatic conditions are the primary cause of these hazards, additional non-climatic variables such as vegetation cover, topography, and the high velocity of runoff also influence floods [23]. In this regard, the area under study is significantly exposed to the risk of flooding due to the high terrain and low infiltration; consequently, it is crucial to identify flash flood hazards in the study area. The study area has poor land vegetation cover, which contributes relatively little to rainfall loss and can, therefore, lead to increased runoff. The spatial distribution of vegetation cover represents less than 1% of the total area (Figure 2a,c). On the other side, it is covered by impervious basement rocks, which belong to group D in the hydrological soil groups (HSGs), quaternary sediments, which belong to group C, and group A, which represents sandy soil, which represents 10% of the area (Figure 2b). According to Helmi & Zohny [24], the study area has a curve number (CN) of 82, indicating that it has a low infiltration and a high probability for runoff. The hydrological problems are related to the risks of flash flooding and lack of rainfall drainage.

Geologically, the study area has attracted the interest of many researchers because it displays most of the structural and rocky aspects of the Precambrian (igneous and metamorphic) rock units that cover Egypt's Central Eastern Desert [25]. The area under investigation is mainly covered by two main rock units: sedimentary rock and pre-Cambrian igneous and metamorphic rock units. Regarding the sedimentary deposits, they are represented in Cretaceous, Tertiary, and Quaternary rocks along the coastal plain of the Red Sea and in wadi floor sediments. The different rock units that build up the investigation area and the structural trends are given through the geologic map after Conoco (1987), as shown

in Figure 3. Structurally, the area was subjected to deformation events affecting the rock units during the Pan African times. Several types of unconformities have been traced in the study area: (1) Late Proterozoic–Cretaceous unconformity (non-conformity type), which separates between the basement and sedimentary rocks. (2) Disconformity type between Eocene and Oligocene rock units, Ranga Formations, and older sediments of Oligocene sediments, Umm Mahara Formation and Ranga Formation, and between Miocene rocks and Quaternary deposits. (3) The Hammamat series unconformably overlies the ophiolitic mélangé rocks and represents the extension of the known Wadi Kareim basin [25]. The study area is cut by different sets of faults including the following: NW–SE (Red Sea–Gulf of Suez trend, E–W (Mediterranean trend)) and NE–SW (the Gulf of Aqaba trend), as shown in Figure 3.



**Figure 2.** (a) Normalized Difference Vegetation Index (NDVI) of the study area, (b) soil map (hydrologic soil groups) of the study area, (c,d) selective locations of field investigation of the study area.

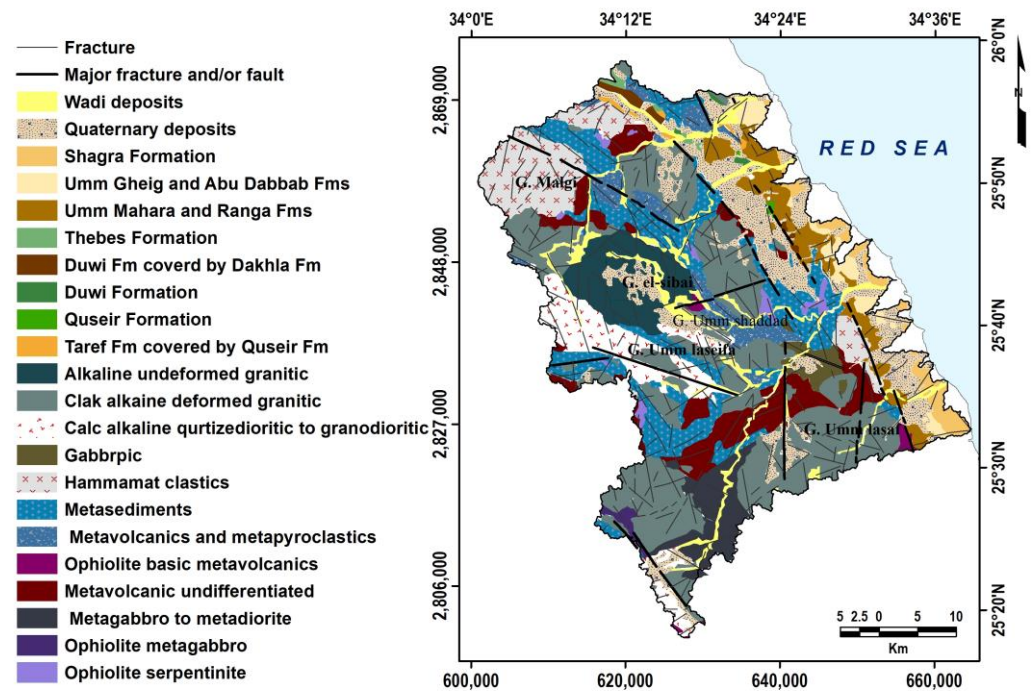


Figure 3. Geologic map of the study area after Conoco [25].

### 3. Methodology

The estimation of hydro-morphometric parameters of the studied basins reflects the research methodology to estimate flash flood hazards (Figure 4). El Shamy’s approach and ranking method are used to assess flood hazards in the study area. In order to achieve these objectives, many effective materials and methods have been used, which include geological and topographic maps, DEM data, and RS data, using ArcGIS 10.2 [26], WMS 11.1 [27], ESA SNAP 9.0 [28], and Google Earth Pro 7.3, [29].

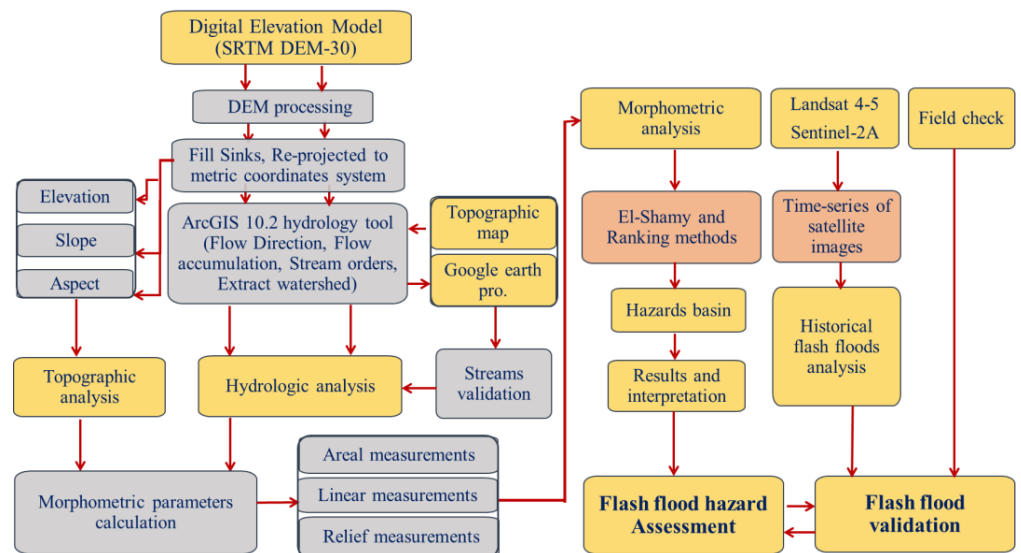


Figure 4. Flow chart outlining the study’s methodology.

Throughout the analysis, topographical maps (EGSA, 1989), with a scale of 1:50,000 covering the area, and a geological map [30], with a scale of 1:500,000 of the study area, were utilized as supports to assessment. Digital Elevation Model, which is derived from Shuttle Radar Topography Mission (SRTM) data, was downloaded from the United States

Geological Survey (USGS) website with 30m spatial resolution. The SRTM DEM data is more accurate vertically and horizontally and is less impacted by weather conditions than DEM derived from optical ASTER [31,32]. SRTM-derived DEM data usually contains many sinks, which are considered anomalous and illogical areas. To minimize errors, this anomaly was corrected and filled using the sink fill algorithm in ArcGIS. Next, the geographic coordinate system of DEM is re-projected to the metric coordinate system using the projection tool to obtain true measurements of the slope and other parameters. The DEM dataset is employed in the current analysis to determine basin boundaries, stream networks, stream orders, and morphometric parameters. The morphometric features of the basins (one-dimensional linear measurements, two-dimensional areal measurements, and three-dimensional relief measurements) are measured using the equations and methods listed in Table 1. The El Shamy [33] approach and ranking method based on the morphometric measurements of the investigated wadis were applied to generate the flash flood hazard map.

(a) El-Shamy approach [33]

In order to identify the hazardous basin, El-Shamy (1992) suggests two different relations. Stream density and mean bifurcation ratio are used to illustrate the first relationship, while mean bifurcation ratio and stream frequency are used to illustrate the second. El Shamy's approach diagrams have three categories (A, B, and C). Class (A) represents wadis with low flood potentiality and a high potential for rainwater recharge to shallow aquifers. Class (C) recognizes basins that have high opportunities for flood risk and low surface water recharge potentialities to shallow aquifers. Finally, class (B) characterizes basins with a medium chance of stormwater recharge potential in shallow aquifers and intermediate probabilities of flood hazards.

(b) Ranking method

The ranking, which is named the linear equation system, is among the most essential tools for flood probability mapping. This method was suggested by Davis [34] for predicting the risk of a flash flood and later updated by several authors. In this method, two linear equations were used to measure the hazard degree of flood in each basin. For the morphometric measurements whose relationship to the flood risk is directly proportional, Equation (1) [34] was applied, while Equation (2) [34] was used for the other morphometric measurements that are inversely related to the degree of hazard.

$$\text{Hazard degree} = \frac{(y_{\max} - y_{\min}) \cdot (X - X_{\min})}{(X_{\max} - X_{\min})} + y_{\min} \quad (1)$$

$$\text{Hazard degree} = \frac{(y_{\max} - y_{\min}) \cdot (X - X_{\max})}{(X_{\min} - X_{\max})} + y_{\min} \quad (2)$$

where the maximum and minimum limits of the suggested hazard scale number are represented by  $y_{\max}$  and  $y_{\min}$ , respectively (from 5, highest, to 1, lowest). The letter  $X$  denotes the value of the previously measured morphometric parameters for the basins, and the maximum and minimum measured values of any morphometric parameter are displayed by  $X_{\max}$  and  $X_{\min}$ . The previous two Equations can be simplified to the following:

$$\text{Hazard degree} = \frac{4 \cdot (X - X_{\min})}{(X_{\max} - X_{\min})} + 1 \quad (3)$$

$$\text{Hazard degree} = \frac{4 \cdot (X - X_{\max})}{(X_{\min} - X_{\max})} + 1 \quad (4)$$

The results of the two approaches were compared to see if they achieve results that are compatible. Also, by integrating the two approaches, the best hazard degree evaluation for any drainage basin is given. The flash flood assessment was verified using satellite images acquired from Landsat 4–5 TM C2 L2 and Sentinel-2A. Landsat data was downloaded from the U.S. Geological Survey (USGS), with a spatial resolution of 30m. However,

Sentinel-2A (European optical satellite launched in 2015) data was downloaded from the European Space Agency (ESA), with a spatial resolution of 10m. ESA created a program (Sentinel Application Platform or SNAP) for processing and analyzing the image of Sentinel satellites. In this regard, flash flood events are examined through four historical satellite images covering the study area through the time from 1994 to 2020. The historical flash flood is of essential importance to validate the flashflood assessment, especially in the absence of the actual measurement of flood hydrograph at the wadi outlet.

#### 4. Hydro-Morphometric Analysis

##### 4.1. Topographic Analysis

The topographic elevation map of the research area (Figure 5a) shows significant variations in topography for the gradient in the elevations from the central part to the other directions. The highest elevation of the area under investigation exists in the central, while the smallest elevation exists in the eastern part of the coastline of the sea. This analysis indicates the terrain elevations range from 0 m, minimum level, to 1452 m, maximum level, above the sea level.

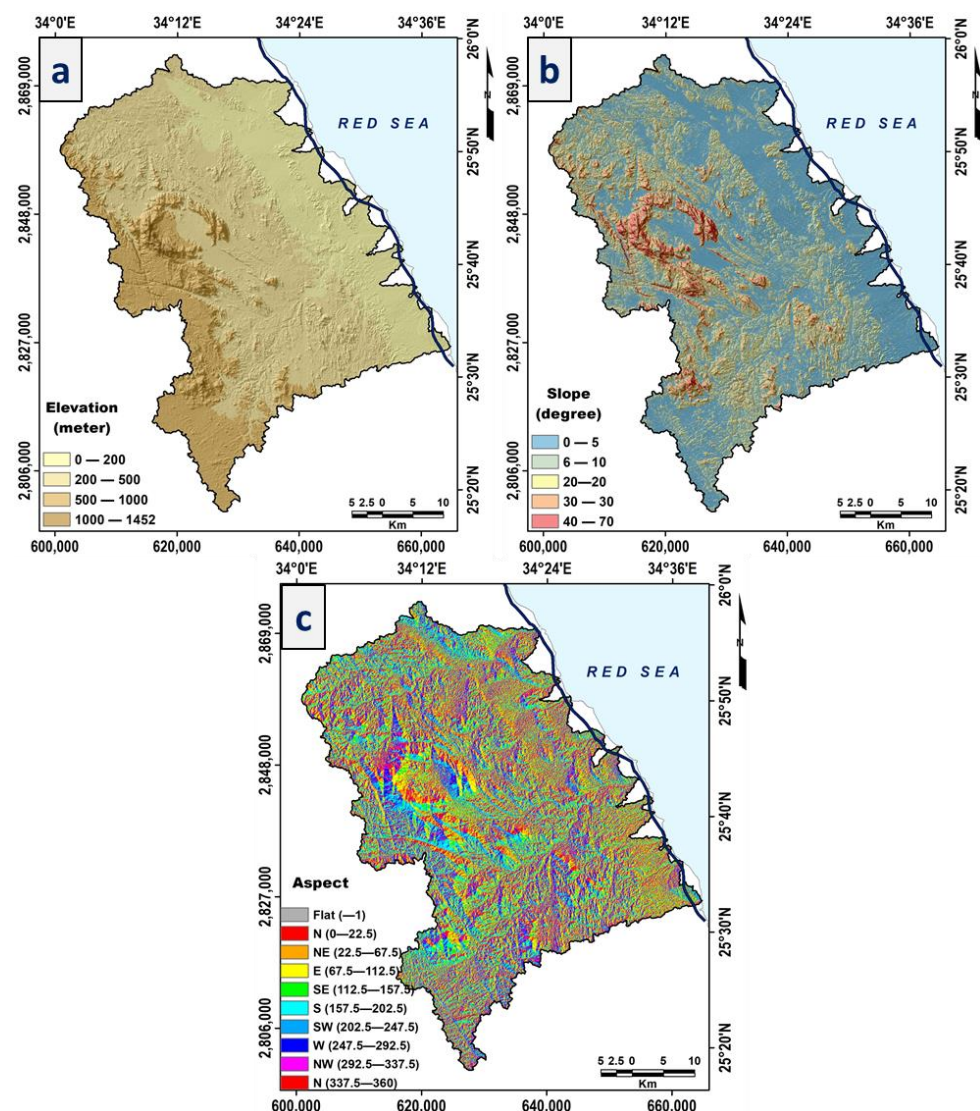


**Figure 5.** Topographic characteristics of the study area. (a) Elevations map of study area extracted from the DEM, (b) degree of the slope derived from the DEM, and (c) the general direction of slopes of the area under investigation.

The slope directly affects the runoff of the rainwater since the high slope increases the velocity of the runoff and then causes flood hazards. In the current study, the coordinate system of the 30m SRTM Elevation Model is re-projected to the metric coordinate system using the projection tool within the GIS environment to obtain true slope measurements. Based on the Zuidam [35] classification (Appendix A, Table A1), the study area's terrain slope ranges from 0 to >30 degrees (Figure 5b). High slope values indicate steeper terrain, while low slope values indicate gentler terrain that may be nearest to flattening. Flash flood activity is increased by these steep slopes that were caused by tectonic activity.

The aspect term means the direction of the slope of any area (Figure 5c). Although two points or pixels may have the same slope degree, one of these pixels may be tilted towards the north direction and another towards the south direction. Considering both aspect and slope together is essential for figuring out the general direction of stream flow.

#### 4.2. Hydrological Analysis

The hydrological database representing flow direction and accumulation, stream networks, and drainage basins has been created for the study area using the ArcGIS hydrology toolbox and DEM. The flow directions are determined for each pixel, where the flow takes the direction from the higher pixel to the lower pixel. The flow accumulation in hydrologic modeling is used to generate the main drain in the basin. To display the other stream networks, the conditional tool within ArcGIS is used to enhance the flow accumulation map. The first step in the quantitative analysis of the basins is to assign stream ordering. There is more than one method of stream ordering systems, such as (a) Horton [36], (b) Strahler [37], and (c) Shreve [38]. The Strahler order is designed to represent the morphology of a basin and has a good mathematical background. The networks of streams in the current study are ordered based on the Strahler method [37].

One of the main problems with the stream network is that the stream path is divided into segments during the stream ordering process. These disconnected streams cause problems in the calculation of morphometric parameters of the basin. Using a GIS environment, the correction was carried out in steps. Therefore, correcting and repairing the disconnected streams must come first before calculating the stream ordering. Through the use of available topographic maps with a scale of 1:50,000 (Appendix B, Figure A1) and Google Earth images, the ordering of the stream networks was verified. The streams, which were automatically extracted using GIS, were imported into Google Earth Pro to visually analyze their position and extension and verify their distribution over the wadis site in the study area. It was noted that one of the streams that were extracted from the GIS is located directly on an old dam that was established in the area of study (Figure 6a). Additionally, the data extracted from topographic maps of selected basins showed that, regarding the stream order, there is an agreement between topographic maps and the DEM, with a rate ranging from 86.2 to 99.4% (Figure 6b).

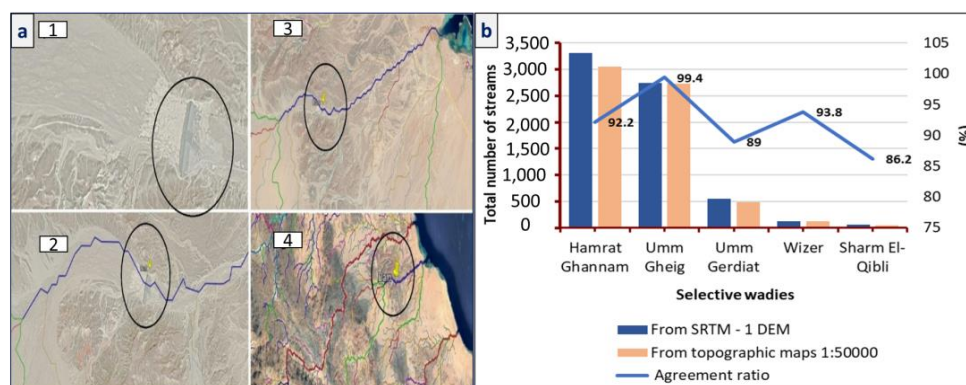


**Figure 6.** Validation of the stream's location and stream ordering using (a1–a4) Google Earth Pro and (b) the results obtained from topographic maps.

As a result, stream networks in the study area reached the 7th order. Each order was discriminated by a different color (Figure 7). In the same context, watershed, catchment, wadi, or drainage basin are terms that mean that an area from the land holds the surface water resulting from rains or any other source and then drains it down to a single point (outlet). The study area has twelve basins that differ in shape and area (Figure 7). Most of these basins are named based on the available topographic maps (Appendix B, Figure A1).

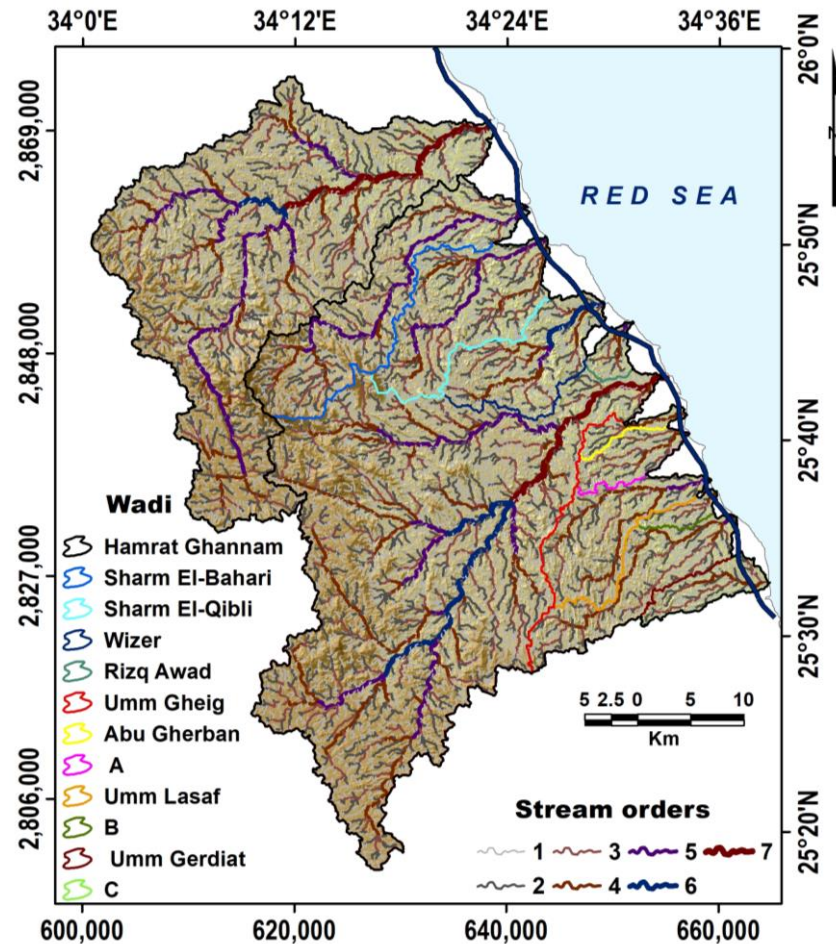


Figure 7. Stream order within the basins of the area under investigation.

#### 4.3. Quantitative Morphometric Analysis

The term “morphometry” refers to the branch of science that is concerned with the quantitative measurements of any natural form’s shape. The pioneer in this field, Horton [36], contributed to this contemporary method of quantitative morphological analysis of the basin. Several geomorphologists further developed and modified Horton’s laws, including Strahler [39,40] and Schumm [41]. These basin’s morphometric parameters can provide information on a basin’s topography, geology, and hydrological behavior. Additionally, it also has a significant impact on the flood peak [42]. In the current study, each basin was highlighted separately to extract its morphometric parameters in detail using ArcGIS and TOPAZ modules in a watershed modeling system (WMS) based on DEM data (Figure 8). As shown in Table 1, the main morphometric parameters of the drainage basins were calculated using the equations and methods. The linear, areal, and relief morphometric characteristics of the basins are summarized in Table 2 and explained below.

**Table 1.** Morphometric parameters selected for the current analysis.

	Morphometric Parameters	Mathematical Expression	References
A		Linear measurements of the drainage watershed	
1	Stream order (Su)	Hierarchical ordering	[37]
2	Stream number (Nu)	$Nu = N1 + N2 + Nn$	[36]
3	Stream length (Lu) km	$Lu = L1 + L2. . . . Ln$	[40]
4	Drainage basin length (Lb)	The longest dimension of the basin, which is parallel to the principal drainage (km)	[41]
5	Average basin width (Wb)	Basin area (A) divided by its length (Lb)	
6	Mean bifurcation ratio (MRb)	MRb = Average of bifurcation ratios Rb of all orders; $Rb = Nu / N(u+1)$ ; Nu is number of streams of any given order, and (u+1) is the next higher order	[36]
7	Length of overland flow (Lg)	$Lg = 1 / (2 \times Dd)$	[36]
B		Areal measurements of the drainage watershed	
1	The area of drainage (A) km <sup>2</sup>	GIS software analysis	[41]
2	Basin perimeter (P) km	Total length of outer boundary of drainage basin	[41]
3	Stream frequency (Fs) km <sup>2</sup>	$Fs = (\Sigma Nu) / A$	[36]
4	Drainage density (Dd) km/km <sup>2</sup>	$Dd = (\Sigma Lu) / A$	[36]
5	Circularity ratio (Rc)	$Rc = 12.57 \times (A / P^2)$	[43]
6	Elongation ratio (Re)	$Re = 2 / Lb \times (A / \pi)^{0.5}$	[41]
7	Form factor (Ff)	$Ff = A / Lb^2$	[36]
8	Infiltration number (If)	$If = Dd \times Fs$	[44]
C		Relief measurements of the drainage watershed	
1	Basin relief (R)	$R = H - h$ ; H is maximum elevation and h is minimum elevation of the basin	[40]
2	Relief ratio (Rr)	$Rr = R / Lb$	[41]
3	Drainage texture (T)	$T = (\Sigma Nu) / p$	[45]
4	Ruggedness number (Rn)	$Rn = R \times Dd / 1000$	[41]
5	Basin Slope (Bs)	WMS software “topaz model”	

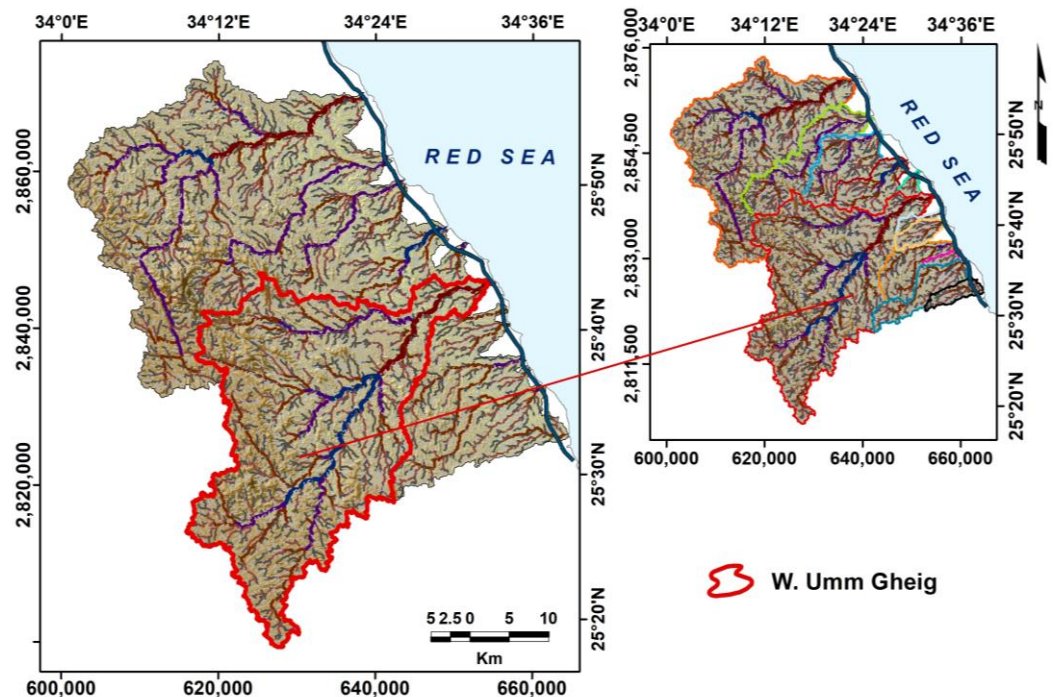


**Figure 8.** A selective example of extracting each basin separately for a detailed study.

**Table 2.** Linear, areal, and relief morphometric parameters of the wadis covering the area under investigation.

W	Linear Morphometric Parameters								Areal Morphometric Parameters										Relief Morphometric Parameters									
	Number of Steams of Each Order								L <sub>u</sub>	L <sub>b</sub>	W <sub>b</sub>	MR <sub>b</sub>	L <sub>g</sub>	A	P	R <sub>e</sub>	R <sub>c</sub>	F <sub>f</sub>	D <sub>d</sub>	F <sub>s</sub>	I <sub>f</sub>	H	h	R	R <sub>r</sub>	T	R <sub>n</sub>	B <sub>s</sub>
	1st	2nd	3rd	4th	5th	6th	7th	N <sub>u</sub>																				
1	1988	475	250	24	5	2	1	2745	1879.7	39.67	16.6	4.30	0.176	660.2	194.2	0.73	0.22	0.42	2.85	4.16	11.9	1450	5	1445	0.036	14.1	4.11	0.171
2	561	143	30	6	1	...	...	741	501.1	31.3	6.0	4.92	0.189	189.0	106.58	0.50	0.21	0.19	2.65	3.92	10.4	1452	0	1452	0.046	6.95	3.85	0.180
3	420	95	25	5	1	...	...	546	351	21.5	6.7	4.56	0.205	143.8	73.60	0.63	0.33	0.31	2.44	3.80	9.3	1056	0	1056	0.049	7.42	2.58	0.100
4	311	71	16	6	2	1	...	407	278.3	17.7	5.7	3.30	0.180	100.4	60.66	0.64	0.34	0.32	2.77	4.05	11.2	417	0	417	0.024	6.7	1.16	0.086
5	51	15	4	2	1	...	...	73	43.0	6.27	2.5	2.79	0.179	15.41	20.27	0.70	0.46	0.39	2.79	4.74	13.2	183	5	178	0.028	3.6	0.5	0.067
6	2522	601	145	31	8	2	1	3310	2560	49.97	17.1	3.82	0.167	855.3	229.63	0.66	0.20	0.34	2.99	3.87	11.6	1349	0	1349	0.027	14.4	4.04	0.170
7	38	6	2	1	...	...	...	47	39.10	10.26	1.5	3.78	0.193	15.07	31.29	0.42	0.19	0.14	2.59	3.12	8.1	210	3	207	0.020	1.5	0.54	0.065
8	98	24	5	1	...	...	...	127	92.4	12.0	3.1	4.63	0.159	36.79	34.97	0.57	0.38	0.26	2.51	3.45	8.7	338	0	338	0.028	3.63	0.85	0.072
9	285	63	12	2	1	...	....	363	242	18.1	5.2	4.44	0.196	94.72	62.54	0.60	0.30	0.28	2.55	3.83	9.8	586	0	586	0.032	5.80	1.50	0.161
10	45	10	2	1	...	...	...	58	30.8	7.96	1.7	3.83	0.223	13.71	22.78	0.52	0.33	0.22	2.25	4.23	9.5	210	0	210	0.026	2.55	0.47	0.043
11	284	66	12	2	1	...	...	365	252.7	24.1	3.96	4.45	0.189	95.48	74.29	0.45	0.21	0.16	2.65	3.82	10.1	620	4	616	0.026	4.91	1.63	0.094
12	101	24	4	1	...	...	...	130	94.0	11.13	3.1	4.74	0.182	34.15	37.83	0.59	0.30	0.28	2.75	3.81	10.5	316	0	316	0.028	3.44	0.87	0.060

where, W, wadi name, 1 = HamratGhannam, 2 = Sharm El-Bahari, 3 = Sharm El-Qibli, 4 = Wizer, 5 = RizqAwad, 6 = Umm Gheig, 7 = Abu Gherban, 8 = A, 9 = Umm Lasaf, 10 = B, 11 = Umm Gerdiat, 12 = C, N<sub>u</sub>, Total number of stream orders, L<sub>u</sub>, Total stream length (km), L<sub>b</sub>, basin length (km), W<sub>b</sub>, Basin width (km), MR<sub>b</sub>, Meanbifurcation ratio, L<sub>g</sub>, Length of overland flow (km), A, Area, P, Perimeter, R<sub>e</sub>, Elongation ratio, R<sub>c</sub>, Circularity ratio, F<sub>f</sub>, Form factor, D<sub>d</sub>, Drainage density, F<sub>s</sub>, Stream frequency, I<sub>f</sub>, Infiltration Number, H, maximum elevation, h, minimum elevation, R, Basin relief in meter, R<sub>r</sub>, Relief ratio m/km, T, Basin texture, R<sub>n</sub>, Ruggedness number, and B<sub>s</sub>, Basin Slope.

#### 4.3.1. Linear Measurements of the Basins

Stream orders (Su) and stream numbers (Nu) are two of the most significant morphometric parameters in morphometric analysis if there are two basins with the same amount of rain falling and have the same area. They may differ in the runoff due to the difference in their stream order. However, the higher the network's stream order, the higher the runoff and, consequently, the higher the risk of flooding. That is because a raindrop takes less time to travel from any point in the basin to the outlet, causing runoff to accumulate quickly and produce a high hydrograph peak. The stream orders of the studied basins range between the 4th and 7th orders. The Wadi A, B, C, and Abu Gherban have the lowest rank (4th order), and the Umm Gheig and Hamrat Ghannam basins have the highest rank (7th order). On the other hand, the total number of streams in the studied basins is the maximum (3310 streams) in Wadi Umm Gheig and the minimum (47 streams) in Wadi Abu Gherban.

Total stream lengths (Lu) differ significantly from one wadi to the other—they depend on the area of the basins and the number of streams. The morphometric analysis indicates that Wadi Umm Gheig is the longest one in terms of total stream lengths of 2560 km, while Wadi B is the shortest one in terms of total stream lengths of 30.8 km. These values varied between basins, indicating a difference in infiltration capacity that might be caused by changes in slope and terrain. The stream's length reveals how climate, vegetation, and rock erosion resistance are related [46]. In the same context, under the same conditions, impervious rocks support longer stream lengths [47].

Basin length (Lb) is defined as the tallest length of the watershed that lies parallel to the mainstream [41]. Gregory [48] described the length of the basin as the tallest pass of the watershed, in which one end of the passage is at the basin's outlet. According to the morphometric analysis, the highest basin length is 49.97 km for watershed Umm Gheig, while the shortest one is for watershed Rizq Awad of 6.27 km.

One important morphometric parameter used to estimate the basin's shape is the width of the basin (Wb). The outcomes of the analysis indicate that the width of the wadis differs widely, from 1.5 km in Abu Gherban to 17.1 km in Umm Gheig.

The bifurcation ratio (Rb) is a dimensionless property, defined as a metric of how branched the hydrographic network [36,39]. Generally, the mean of all the bifurcation ratios of the basin (MRb) falls between the value of 2 for basins that are flat terrain and 3–4 for basins that are mountainous [36]. The MRb of the basins covering the study area ranges from 2.79 for Rizq Awad to 4.92 for Sharm El-Bahari. According to Zuchiewicz [49], the higher MRb is a result of the region having recently been exposed to tectonic uplift. On the other hand, basins with lower MRb tend to have experienced fewer structural disturbances [40], and the geological or structural control has not distorted their drainage pattern [41,50]. In this regard, Strahler [40] mentioned that areas with narrow valleys confined between steeply dipping rock might be expected to have an abnormally high MRb. Generally, MRb in the study area is relatively high when they are higher than the suggested normal range by Horton [36] due to structure distortions. From the viewpoint of flood risk, a higher MRb value denotes a slow run of rainwater that allows water to penetrate under the surface, reducing runoff and flash floods [51].

The overland flow length (Lg), which is significantly influenced by infiltration through the soil, is the distance that rainwater travels above the land surface before being accumulated in the basin's stream channels. It has an opposite relationship with flash flood hazards and a direct relationship with infiltration rate [7]. The basins of the study area have a length overland flow with values ranging from 0.159 km of wadi A to 0.223 km of wadi B. Lower Lg values mean a shorter flow distance, which indicates runoff will accumulate more quickly and arrive at the outlet in less time, increasing the risk of flooding.

#### 4.3.2. Areal Measurements of the Basins

Watershed area (A): According to Strahler [37], wadis having the same area and form characteristics have similar geomorphological properties. The outlined area of the basins

covering the study area ranges between 855.3 km<sup>2</sup> in the Umm Gheig basin and 13.71 km<sup>2</sup> in basin B. Generally, assuming that infiltration, slope, and precipitation are the same for two watersheds, a watershed with a large area will receive a large amount of rains, and thus will cause significant runoff and may result in high hazard. Horton (1932) classified the basins on the basis of their surface area into three groups: the larger e basin > 100 km<sup>2</sup>, the medium basin ranged from 50 to 100 km<sup>2</sup>, and the smaller basin < 50 km<sup>2</sup>. The study area watersheds fall into the small to large area category.

The watershed perimeter (P) represents the outer frame of the watershed that separates it from other adjacent basins. The basins' perimeter varies greatly from one to another, ranging from 20.27 km in Rizq Awad to 229.63 km in Umm Gheig.

The basin shape mainly reflects how surface water will flow out of the basin. The circular basins, which differ from elongated ones, will cause runoff from different directions of the wadi that reach the mainstream at roughly the same time. In this regard, the circular basin is characterized by a large drain in a shorter amount of time [52,53] additionally, the flooding peak is higher than the elongated one. Accordingly, the elongated basins have less runoff possibility [54], which takes their chance to infiltrate, and also, the runoff will spread out over time. Hence, the elongated basins are simpler to manage and control than the circular basins, and their waters have a higher probability of infiltration into the water table [55]. The ratio of elongation, ratio of circulatory, and shape factor represent the three key indices used to assess basin shape.

The elongation ratio (Re), according to Schumm [41], measures the shape of the catchment and ranges from 0 to 1, where a value of 0 indicates that the catchment is highly elongated and a value of 1 indicates that it is circular. An Re near one is typical for areas that have low relief, while  $Re < 0.8$  is assumed to be elongated and is typically connected to steep slopes and moderate to high relief [40]. In general, basins with an elongation ratio of <0.7 reflect that the lag time is longer and that flooding hazards are consequently reduced [17,40,54]. The morphometric analysis results indicate that the basins in the area of study have elongation ratios that range between 0.42 and 0.73 for Wadi Abu Gherban and Wadi Hamrat Ghannam, respectively. According to the standard classification of the basin shape given in (Appendix A, Table A2), the study area's basins tend to be elongated in shape.

Miller [43] described the circularity ratio (Rc) as the ratio of the catchment's surface area to the surface area of a circle with the same perimeter as the catchment. The Rc varies from 0 to 1. If it is close to or equal to 1, the catchment is circular in shape, while the catchment is elongated in shape if the Rc is closer to zero. The morphometric analysis results indicate that the Rc of the basins covering the study area ranges from 0.19 for Abu Gherban to 0.46 for Rizq Awad. In this context, the lower circularity ratio of the basins means that they are close to the elongated in shape.

The form factor (Ff) parameter was suggested by Horton [36], and it can be measured as the ratio between the surface area of the watershed and its length squared. Ff values range from 0 to 1. A higher Ff suggests that the watershed is close to being circular in shape, while a lower value suggests that the watershed is close to being elongated. The results of the analysis indicate that the drainage basin's form factor ranged from 0.14 for Wadi Abu Gherban to 0.42 for Wadi Hamrat Ghannam. It indicates that the shape of basins that cover the area of study tends to be elongated.

Drainage density (Dd) indicates how far apart or close the streams are within the basin [40]. Eze and Efung [56] reported that low drainage density denotes fractured hard rocks, suggesting that a large percentage of rainstorms will infiltrate to recharge the aquifer, while high drainage density suggests great runoff of precipitation. In the present study, the Dd differed from 2.25 km/km<sup>2</sup> for wadi B to 2.99 km/km<sup>2</sup> for Umm Gheig. Accordingly, these basins have poor drainage and have a rough texture. When comparing basement rocks, the granite of the central Eastern Desert has a lower mean drainage density, and thus, basins with lower Dd are better for groundwater storage.

Stream frequency or channel frequency ( $F_s$ ), described by Horton [36], is the total number of channels in a network of all orders in a watershed per unit area. The stream frequency differs from one to 6 or maybe more based on the basin lithology. In the current study,  $F_s$  ranges from 3.12 to 4.74 streams per  $\text{km}^2$  for Wadi Abu Gherban and Rizq Awad, respectively. As a result, the basins covering the study have relatively moderate stream frequency, which means they represent moderate surface runoff because it means the basin keeps an amount of water without draining.

The infiltration number ( $I_f$ ), which depends on stream density and frequency, gives useful information on the basin's infiltration characteristics. A low drainage density and frequency increases soil infiltration capacity [57]. The infiltration number is directly related to the runoff potential and inversely related to the infiltration [40]. The results reveal that the infiltration of the study area ranged between 8.1 (Wadi Abu Gherban) and 13.2 (Wadi Rizq Awad). As a result, the surface runoff increases in the Wadi Rizq Awad more than in the other—this means a high hazard.

#### 4.3.3. Relief Characteristics of the Drainage Watersheds

Basin Relief ( $R$ ): According to the study results, the basin relief varies greatly between 207 m for Abu Gherban and 1452 m above sea level for Sharm El-Bahari. As an outcome, the relief of basins covering the area under investigation ranges from high to very high as the erosional forces are relatively greater. According to Kadam et al., [58], the basin with higher relief leads to the high gravity of rainfall flow, less soil penetration conditions, and great surface runoff.

The relief ratio ( $R_r$ ) is a significant factor for measuring a watershed's general slope [59]. According to Schumm [41],  $R_r$  has a direct relationship with flash floods and an inverse relationship with concentration time. Abdelkader et al., [47] reported that the watersheds that cover the basement and Tertiary rocks contain high  $R_r$  values. The relief ratio in the present study, according to the morphometric measurements, differs from 0.020 m/km to 0.049 m/km for the Wadis Abu Gherban and Sharm EL-Qibli, respectively. Generally, lower  $R_r$  indicates the slope of the wadi is light; thus, runoff will decrease, while larger  $R_r$  indicates the slope of the wadi is steep; thus, runoff will increase.

Drainage texture ( $T$ ), an essential element of the morphometric measurements, is significantly influenced by soil type, relief aspect, and infiltration [60]. It is useful in describing how close or far away the streams are from each other and thus indicates the texture of the terrain. The study revealed that the texture ratio in Wadi Abu Gherban and Wadi Umm Gheig, respectively, ranges from 1.5 to 14.4 km. Based on Smith's classification [45] (Appendix A, Table A3), the studied basins are listed under the very fine to very coarse texture category. According to Smith [45] and Sujatha et al., [61], fine drainage texture appears in soft rocks or permeable surfaces without vegetation cover, while coarse drainage texture appears in hard rocks or impermeable soil.

The ruggedness number ( $R_n$ ) of the watersheds covering the area under investigation varies between 0.47 and 4.11 in basin B and Hamrat Ghannam, respectively. Based on Melton [62], the high  $R_n$  implies a rough topography, complex structural features in the area, and high drainage density. It means that high  $R_n$  values may cause an increase in watershed peak discharge.

Basin Slope ( $BS$ ), one of the main morphometric measurements, is essential in assessing the risk of flooding as surface water flows along the direction of a steep slope. The basins' slope was calculated using the WMS software's TOPAZ model and varies from 0.043 to 0.180 for basin B and basin Sharm El-Bahari, respectively. In steep basin slopes, water infiltration is low, and overland flow velocity is high; it means faster runoff and the possibility of flood hazards. Basins with higher slopes have rapid runoff volume and potential soil erosion.

## 5. Results and Discussion

The study drainage basins are characterized by their small area (13.7 to 855.3  $\text{km}^2$ ). It reflects that a single rainstorm often covers all the study basins, and this happened during

the rainstorms that occurred in 2016 and in 2020 when the storm covered large areas of Egyptian territory and the resulting flash floods in many large basins in Egypt. On the other hand, there are no sufficient measurements of rainstorms. As the nearest rain gauge station is located 20 km north of the study area and the other stations are far away, they do not represent the real storm affecting the study wadis. In this regard, many efforts were focused on investigating a single large basin containing a number of sub-basins. The current study focused on studying the flood risks of a group of basins that cross the area located on the Red Sea coast to protect roads and facilities. The wadis of the study area are classified as ungauged wadis systems. However, the general lack of actual measurements of flash floods is due to difficulty of access or lack of funding. Understanding of the runoff system is limited by the lack of rainfall/discharge measurements at the outlet. Consequently, the hydrological modeling of these wadis at this time is quite empirical [63]. Additionally, numerous large flood events occurred but were not reported, displaying the insufficiency of the hydrological data available at the time for planning [63]. Subsequently, the hydrogeomorphological parameters play an effective role in assessing the risk of floods. In this context, the flash flood estimate was verified based on the field check and historical flash floods derived from satellite images due to the difficulty and absence of real measurements of runoff hydrograph at the wadi outlet.

### 5.1. Assessment of the Risk from Floods Using Morphometric Parameters

#### 5.1.1. El-Shamy's Approach for Assessment of the Risk of Floods

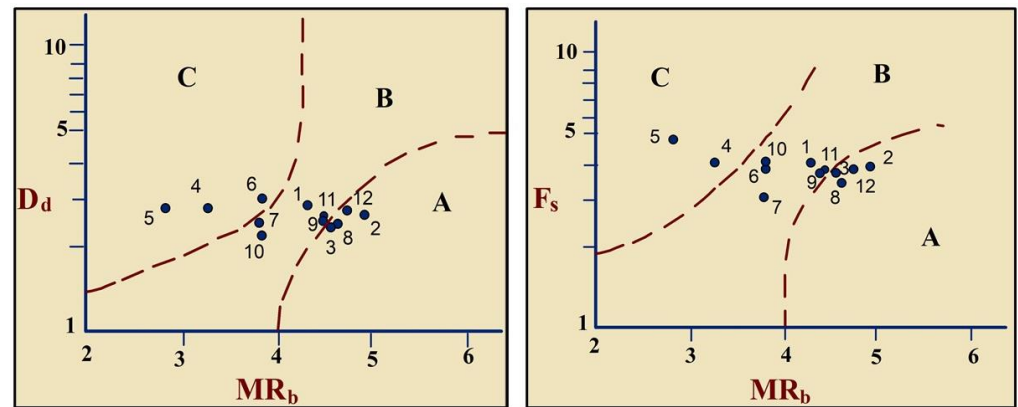
In the current analysis, three key morphometric parameters, MRb, Dd, and Fs, of the studied basins are graphically plotted on the El-Shamy [33] diagram cross-plots (Figure 9). These parameters determine the relationship between flooding and the recharge potential of the groundwater. However, low Fs or Dd and high MRb values contribute to low probabilities of flood risk and high aquifer recharge potentialities. Likewise, high Fs or Dd and low MRb values help to provide a high probability of flooding risk and low surface water recharge potentiality to shallow aquifers. However, with the increasing drainage density and drainage frequency, the decreasing elongation, hence the flood probability increases.

As indicated by the MRb and Dd relationship diagram (Figure 9), the wadis covering the study area have the possibility of flood, ranging from low to high (Figure 10a). Wadis No. 2 (Sharm El-Bahari), 3 (Sharm El-Qibli), 8 (A), and 12 (C) fall in class A, suggesting that they have a lower probability of flash floods. Likewise, wadis No. 1 (Hamrat Ghannam), 7 (Abu Gherban), 9 (Umm Lasaf), 10 (B), and 11 (Umm Gerdiat) spread in class B, reflecting moderate flash flood hazardous probabilities, while wadis 4 (Wize), 5 (Rizq Awad), and 6 (Umm Gheig) have high susceptibility to flooding and fall in class C. In the same context, as indicated by the MRb and Fs relationship diagram (Figure 9), the wadis within the study area have a possibility of flood, ranging from low to high (Figure 10b). Wadis No. 2 (Sharm El-Bahari), 3 (Sharm El-Qibli), 8 (A), and 12 (C) fall in class A, displaying that they have a lower chance of flash floods. Finally, wadis No. 1 (Hamrat Ghannam), 6 (Umm Gheig), 7 (Abu Gherban), 9 (Umm Lasaf), 10 (B), and 11 (Umm Gerdiat) spread in class B that reflect moderate flash flood hazardous probabilities, and only wadis 4 (Wizer) and 5 (Rizq Awad), have a high susceptibility to flooding and fall within class C.

#### 5.1.2. The Ranking Method for Assessment of the Risk of Floods

In the current analysis, thirteen morphometric parameters were selected to assess the hazard; these parameters affect the flood directly, according to Abduladheem et al., [57]. These parameters include (1) area, circulation ratio, drainage density, elongation ratio, stream frequency, form factor, relief ratio, basin slope, total stream length, infiltration ratio, and ruggedness number; (2) length of overland flow and bifurcation ratio. The flooding hazard degree is directly proportional to morphometric parameter number 1 (where the degree of risk is higher for the higher parameter value) and inversely proportional to morphometric parameter number 2 (where the lower MRb and Lg values reflect the

higher runoff; thus, higher hazards). The total flood hazard degree for morphometric measurements of wadis is listed in Table 3.



- 1 = HamratGhannam      4 = Wizer      7 = Abu Gherban      10 = B
- 2 = Sharm El-Bahari      5 = RizqAwad      8 = A      11 = Umm Gerdiat
- 3 = Sharm El-Qibli      6 = Umm Gheig      9 = Umm Lasaf      12 = C

**Figure 9.** Hydro-geomorphometric charts showing lash flood possibilities based on the  $MR_b$  versus  $D_d$  and  $MR_b$  versus  $F_s$  using El Shamy’s approach [33].

**Table 3.** Shows the degree of flood hazard for the catchment based on the morphometric parameters using the ranking method.

Wadi	A	Re	Rc	$F_f$	$D_d$	$F_s$	$R_r$	$R_n$	Bs	LU	$I_f$	$MR_b$	$L_g$	Sum of Hazard	Hazard Degree
1	4.1	5.0	1.4	5.0	4.2	3.6	3.2	5.0	4.7	3.9	3.9	2.2	3.9	50	5
2	1.8	2.0	1.3	1.7	3.2	3.0	4.6	4.7	5.0	1.7	2.8	1.0	3.1	36	3
3	1.6	3.7	3.1	3.4	2.0	2.7	5.0	3.3	2.7	1.5	1.9	1.7	2.1	35	3
4	1.4	3.8	3.2	3.6	3.8	3.3	1.6	1.8	2.3	1.4	3.4	4.0	3.7	37	3
5	1.0	4.6	5.0	4.6	3.9	5.0	2.1	1.0	1.7	1.0	5.0	5.0	3.8	44	4
6	5.0	4.1	1.1	3.9	5.0	2.9	2.0	4.9	4.7	5.0	3.7	3.1	4.5	50	5
7	1.0	1.0	1.0	1.0	2.8	1.0	1.0	1.1	1.6	1.0	1.0	3.1	2.9	20	1
8	1.1	2.9	3.8	2.7	2.4	1.8	2.1	1.4	1.8	1.1	1.5	1.5	5.0	29	2
9	1.4	3.3	2.6	3.0	2.6	2.8	2.7	2.1	4.4	1.3	2.3	1.9	2.7	33	3
10	1.0	2.3	3.1	2.1	1.0	3.7	1.8	1.0	1.0	1.0	2.1	3.0	1.0	24	1
11	1.4	1.4	1.3	1.3	3.2	2.7	1.8	2.3	2.5	1.4	2.6	1.9	3.1	27	2
12	1.1	3.2	2.6	3.0	3.7	2.7	2.1	1.4	1.5	1.1	2.9	1.3	3.6	30	2

Relative hazard degree: 1 = low; 2 = slightly; 3 = moderate; 4 = high; 5 = very high. 1 = HamratGhannam; 4 = Wizer; 7 = Abu Gherban; 10 = B; 2 = Sharm El-Bahari; 5 = Rizq Awad; 8 = A; 11 = Umm Gerdiat; 3 = Sharm El-Qibli; 6 = Umm Gheig; 9 = Umm Lasaf; 12 = C.

The hazard degree summation for the studied wadis was measured, and the results show that it ranges from 24 to 50 for wadi B and both wadis Hamrat Ghannam and Umm Gheig, respectively (Table 3). The relative hazards for basins were ranked based on the estimated and summed hazard degrees. Each basin has a hazard scale number that has been specified. Thus, the basins with hazard degrees of 1, 2, 3, 4, and 5 are weakly, slightly, moderately, highly, and very highly hazardous, respectively. To create the flood hazard map within the ArcGIS environment for the ranking morphometric parameters, three levels of flooding hazard susceptibility were used to classify the relative hazard degree for the 12 basins: low, moderate, and high degrees (Figure 10c). Subsequently, the degree of flood hazards in the wadis covering the area under investigation ranges from low to high as follows: (1) low (wadi Abu Gherban, wadi A, wadi B, Wadi Umm Gerdiat, and wadi C), (2) moderate (Wadi Sharm El-Qibli, Wadi Sharm El-Bahari, Wadi Wizer, and Wadi Umm Lasaf), and (3) high (Wadi Hamrat Ghannam, Wadi Rizq Awad, and Wadi Umm Gheig).

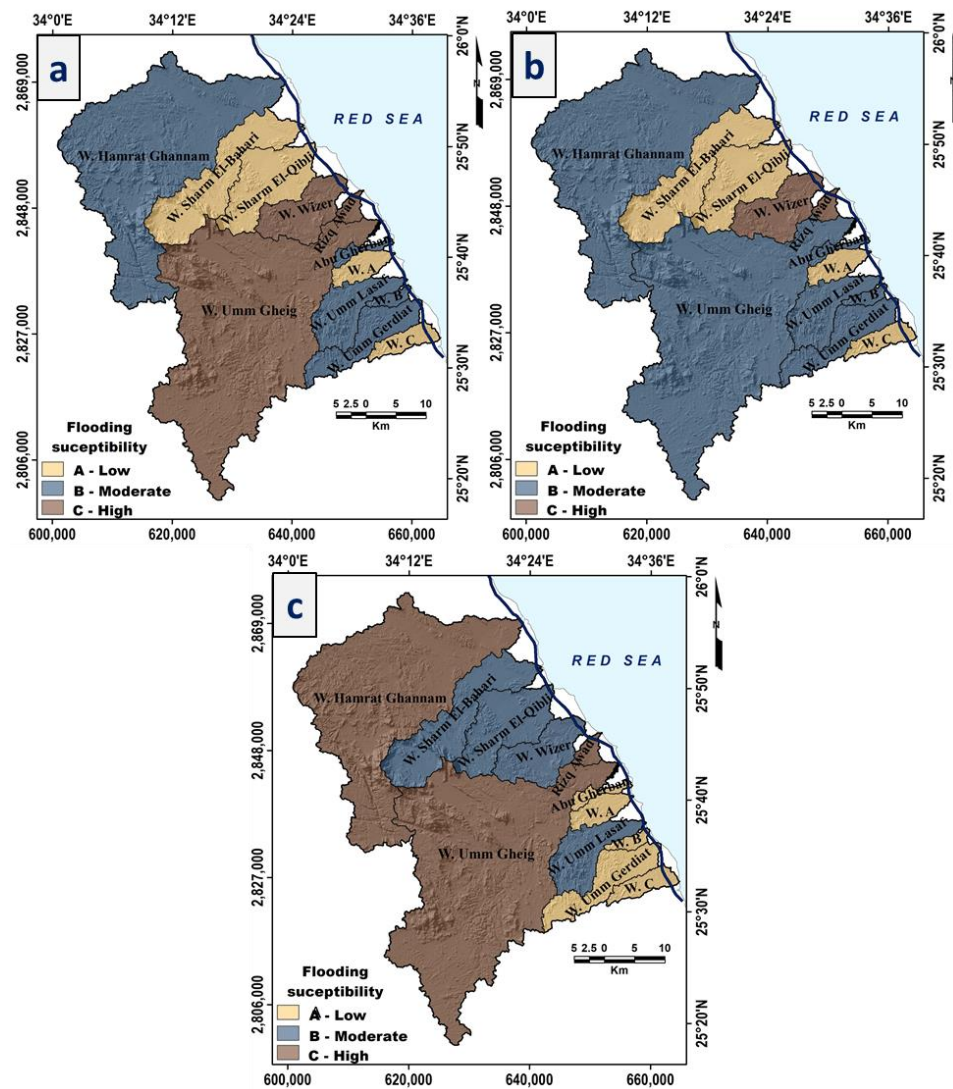


**Figure 10.** Flooding susceptibility map obtained by (a) El-Shamy’s diagram ( $MR_b$  versus  $D_d$ ), (b) El-Shamy’s diagram ( $MR_b$  versus  $F_s$ ), and (c) the ranking method.

Based on the El-Shamy approach and ranking method, the outcome results correlated, as listed in Table 4. It indicates that Wadis Sharm El-Qibli, Sharm El-Bahari, A, and C are ranked under low susceptibility to flooding. Similarly, the Wadis of Hamrat Ghannam, Abu Gherban, Umm Lasaf, Umm Gerdiat, and wadi C are rated as having a moderate susceptibility to flooding. Equally, the wadis of Wizer, Rizq Awad, and Umm Gheig are classified as having a high risk of flooding. The study is limited by the digital elevation model that was obtained, as there was no small-scale land surveying available for the study area. The area of study, which is a mountainous region covered by the Red Sea mountain ranges, has been less affected by changes in land cover and land use throughout past years.

**Table 4.** Classification of wadis’ susceptibility to flooding based on El-Shamy’s approach and ranking method.

Watershed	El-Shamy’s Approach ( $MR_b$ vs. $D_d$ )	El-Shamy’s Approach ( $MR_b$ vs. $F_s$ )	Ranking Method
Hamrat Ghannam	Moderate	Moderate	High
Sharm El-Bahari	Low	Low	Moderate
Sharm El-Qibli	Low	Low	Moderate
Wizer	High	High	Moderate
Rizq Awad	High	High	High
Umm Gheig	High	Moderate	High

Table 4. Cont.

Watershed	El-Shamy's Approach ( $MR_b$ vs. $D_d$ )	El-Shamy's Approach ( $MR_b$ vs. $F_s$ )	Ranking Method
Abu Gherban	Moderate	Moderate	Low
A	Low	Low	Low
Umm Lasaf	Moderate	Moderate	Moderate
B	Moderate	Moderate	Low
Umm Gerdiat	Moderate	Moderate	Low
C	Low	Low	Low

### 5.2. Flash Flood Verification

In terms of flash flood assessment, there are two main types of wadi systems, like gauged and ungauged wadi streams. In gauged wadis, there is a gage station that measures the flood flow at the wadi outlet, while in ungauged wadi streams, there is no gage station at the wadi outlet. The Egyptian's wadi system along the Red Sea is ungauged, resulting in a lack of observations of flash floods. Due to the shortage of instrumented catchments, several indirect methods and models have been proposed around the world in an attempt to measure the probability of flooding and flood hazards based on morphometric, metrological, topographic, and geological characteristics. The actual measurements of the wadi flow hydrograph to validate the data, which are generally difficult, are the basis for determining the credibility of these models [64]. On the other side, when field data is difficult to get, remote sensing data are extremely important. In this regard, the current study employs remote sensing satellite imagery data to verify the flash flood assessment. Based on the timeseries of satellite images that were taken close to the flood event for a typical dryland wadi, the flash floods were identified and assessed [65].

When rainwater reaches the ground surface, part of the water may evaporate, and another part may infiltrate into the soil depending on land use/land cover type. The remaining water, after evaporation and infiltration, runs to the surface, causing surface runoff. The difference in time between the starting of runoff and the arrival to peak discharge is commonly short. Next, the peak flow hydrograph is followed by a rapid runoff velocity drop. Fine sediments (slack-water sediments or clay drapes) accumulated and deposited on the surface of the wadi's channels during runoff recession. The grain-size distribution of these deposits is dominated by sediments like sand, silt, and clay, which were sourced from flood water's suspended sediment load [65]. The existence and quantity of fine-grained sediment sources (such as granite and sandstones) within the watershed, as well as the transporting conditions, control the forming of slack-water deposits [66]. The fine sediments, which were deposited during the last stages of flood recession, have a higher reflectivity, and it can be traced from satellite images through the historical flash flood over the study area. For verification, this approach can potentially be used on a dryland catchment [67,68].

Four available satellite images collected in 1994, 2016, 2017, and 2020 effectively monitored the existence of recent runoff (Appendix B, Figure A2). For mapping purposes, the achieved satellite image bands were combined using nature-color composites of bands 4, 3, and 2. The visual examinations of historical images of Landsat 4–5 and Sentinel-2A from 1994 to 2020 for the study area demonstrate the existence of a number of large flash flood events. In this context, the runoff was suggested by the brightness of bed materials within the wadi channel. This brightness results from an increase in spectral reflectance caused by the deposition of fine sediments within the wadi stream. Two selective examples show a change in spectral reflectance from flood event time to short after. Spectral reflectance lowers over time as a result of the residual fine sediments that accumulated and deposited during the recession stage of a flash flood eroded over time after the flood occurrence (Figure 11). In contrast to the wadi path to the surroundings, the spectral signatures reveal contrasting brightness. Hence, it is simple to identify and map channels that have recently undergone flow. In this context, analyzing the historical flash floods of the research area helped to validate the flood hazard assessment resulting from the current study. As a

result, the hazardous wadis displayed a significant spectral reflection, suggesting that fine sediments were deposited during the last stages of flood recession (Figures 12 and 13). Additionally, the field check revealed that the road was damaged significantly at the outlet of the hazardous basins, reflecting a strong flash flood effect (Figure 14a). In the same context, the impact of these floods can be traced by observing the erosion caused by these floods at the base of the wadi's sides (Figure 14b). On the other hand, over the flood events, the low-risk valleys did not exhibit this characteristic to the same extent (Figure 15). As a result, the historical flash floods are essential to validate the flood assessments when it is difficult to actually measure the runoff hydrograph at the outlet of the wadi system.

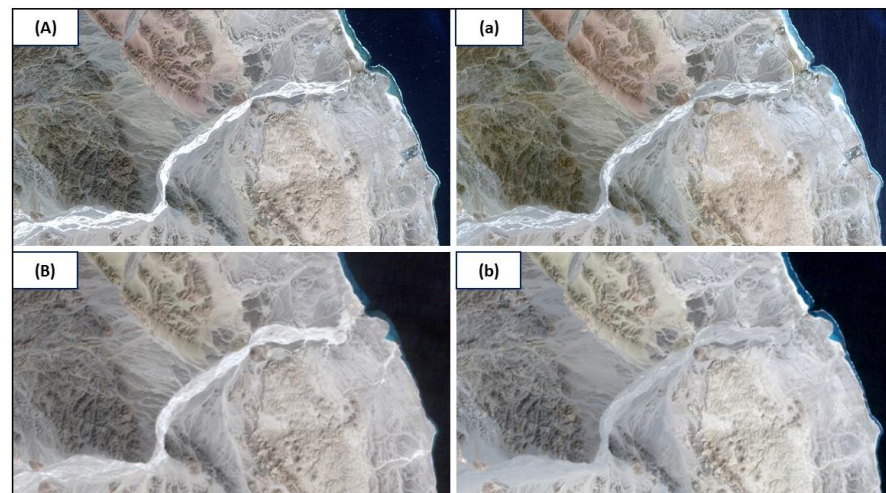


**Figure 11.** Selective examples of two flood events, 2016 (**above**) and 1994 (**down**) of Wadi HamratGhannam, show spectral reflectance lowers with time from flood events (**A,B**) to short after (**a,b**).



**Figure 12.** Displays a significant spectral reflection of Wadi HamratGhannam flow channel, suggesting the fine sediments were deposited during the last stages of flood recession through four historical flood events.

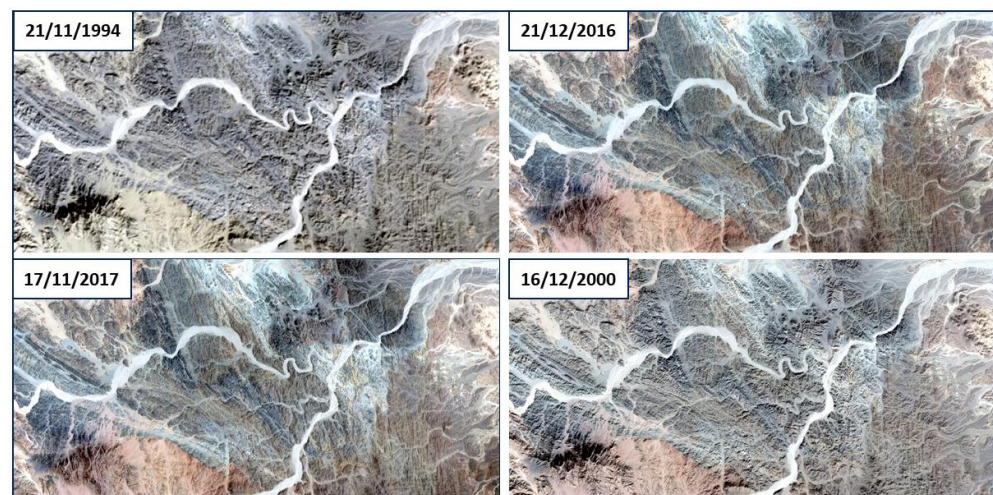


**Figure 13.** Exhibits a significant spectral reflection of Wadi Umm Gheig flow channel, suggesting the fine sediments were deposited during the last stages of flood recession through four historical flood events.



**Figure 14.** Selective examples of flood validation through field observation (a) damage to the road at the outlet of the Wadi Umm Gheig. (b) Flood impact on the undercutting of 4 m terraces in the Wadi Umm Gheig.

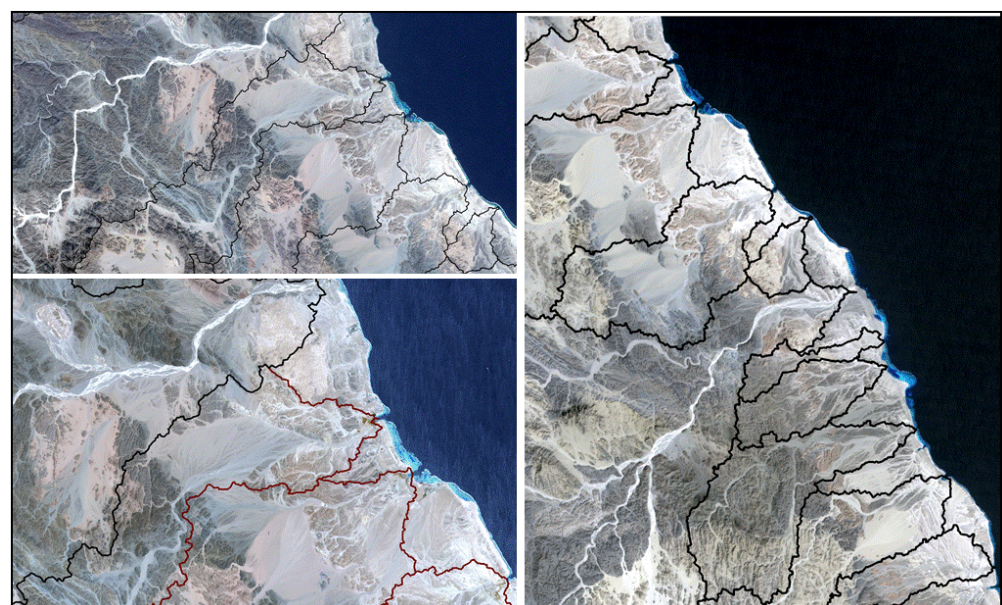


**Figure 15.** Selective example exhibits the difference in spectral reflection degree of wadis with different hazard degrees.

## 6. Conclusions

The current study used ranking and El-Shamy's approach based on hydro-morphometric measurements of the studied basins to assess flash flood hazards. ArcGIS and remotely sensed satellite data images are effectively employed in the measurement of hydrological and morphometric data sets of 12 investigated drainage basins covering the study area. These measurements include linear, areal, and relief characteristics to assess the flash flood hazard. The results of the morphometric measurements show that the study area's basins are divided into small- to large-area categories. The circulation ratios of the watersheds range from 0.19 in basin Abu Gherban to 0.46 in basin Rizq Awad. It indicates that the basins that cover the area of study tend to be elongated in shape and easier to control and manage. The infiltration number (If) indicates the surface runoff increases in the Hamrat Ghannam basin more than the other; this means a high hazard. The integration and matching between El-Shamy's approach and ranking method gives valuable results for evaluating flood hazards. Based on El-Shamy's approach and ranking method, Wadi Wizer, Wadi Rizq Awad, and Wadi Umm Gheig were ranked under high flooding susceptibility. However, the Wadis of Hamrat Ghannam, Abu Gherban, Umm Lasaf, Umm Gerdiat, and wadi C are rated under moderate flooding susceptibility. As for other wadis, they are classified as having a low susceptibility to flooding. The suggested model was validated using field check and satellite images (Landsat 4–5 and sentinel-2A), where they indicated that historical flash floods have occurred in the hazardous wadis. Accordingly, the study area has the probability of flooding that could cause serious environmental hazards, especially since the area contains tourist resorts, urban areas, man-made activities, vital facilities such as Marsa Alam International Airport, and infrastructures such as Red Sea Coastal Road. Accordingly, establishing new urban communities or implementing new projects in the Red Sea region should take this environmental impact into account.

There are several solutions to protect the area under investigation from hazards of flooding and great benefit of rainwater by using one or more solutions from the following: (1) Detention of the accumulated rainwater by building a number of dams along the main streams of wadis to minimize the flooding flow. (2) Crossing the flood water by creating a number of culverts or channels at the outlet of wadis that cut the highway road. These channels must connect the wadi mouth and the Red Sea in order to enable the stormwater to flow into the sea, thus protecting this road from the damage of flood attacks. (3) diversion of wadi pass away from the important facilities by constructing new channels to transfer the water from the mainstream to other places by means of these channels. (4) Storage of the accumulated rainwater for use in various purposes such as drinking and agriculture. Also, surface rainwater that is stored can be injected into the aquifer to prevent it from evaporating and improve groundwater quality, then re-extract it in the future. Finally, the new vital facilities, industrial cities, and urban communities must be built away from the flooding path.

**Author Contributions:** Conceptualization, Adel K. Mohamed and Mohamed Rashwan; methodology, Lamees Mohamed and Mohammed Khattab; software, Mohammed Khattab and Mohamed Rashwan; validation, Fahad Alshehri and Mohamed Rashwan; formal analysis, Sattam Almadani; investigation, Fahad Alshehri; resources, Sattam Almadani; data curation, Mohammed Khattab; writing—original draft preparation, Lamees Mohamed; writing—review and editing, Mohamed Rashwan; visualization, Mohammed Khattab and Lamees Mohamed; supervision, Mohamed Rashwan and Fahad Alshehri; project administration, Adel K. Mohamed; funding acquisition, Fahad Alshehri. All authors have read and agreed to the published version of the manuscript.

**Funding:** This research was funded by the Deputyship for Research & Innovation, Ministry of Education in Saudi Arabia, through project no. IFKSURC-1-7304.

**Data Availability Statement:** The data are not publicly available due to further research.

**Acknowledgments:** The authors extend their appreciation to the Deputyship for Research & Innovation, Ministry of Education in Saudi Arabia, for funding this research work through project no. IFKSURC-1-7304.

**Conflicts of Interest:** The authors declare no conflict of interest.

## Appendix A

**Table A1.** Slope classification modified after Zuidam [35].

Slope Class	Description
0–2	Flat
2–8	Gentle
8–16	Slightly steep
16–30	Steep
>30	Very steep

**Table A2.** Standard and classification of the basin elongation proposed by Schumm [41] and later interpreted by Strahler [40].

Elongation Ratio	Shape of Basin
<0.70	Elongated
0.70–0.80	Less elongated
0.80–0.90	Oval
>0.90	Circular

**Table A3.** Texture rate Classification based on Smith [45] and Vittala et al., [67].

Texture Value	Texture Degree
<2	Very coarse texture
2–4	Coarse texture
4–6	Moderate texture
6–8	Fine texture
>8	Very fine texture

## Appendix B

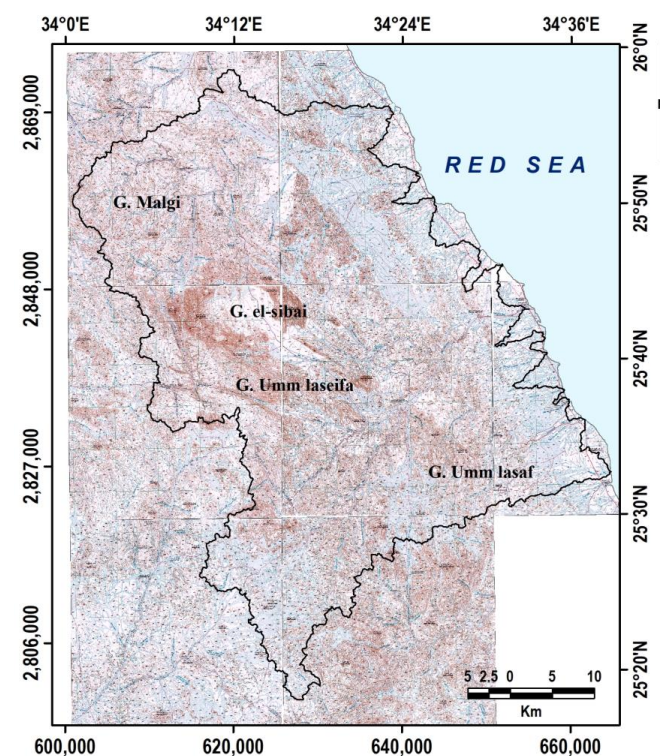


**Figure A1.** Topographic maps of the study area [30].

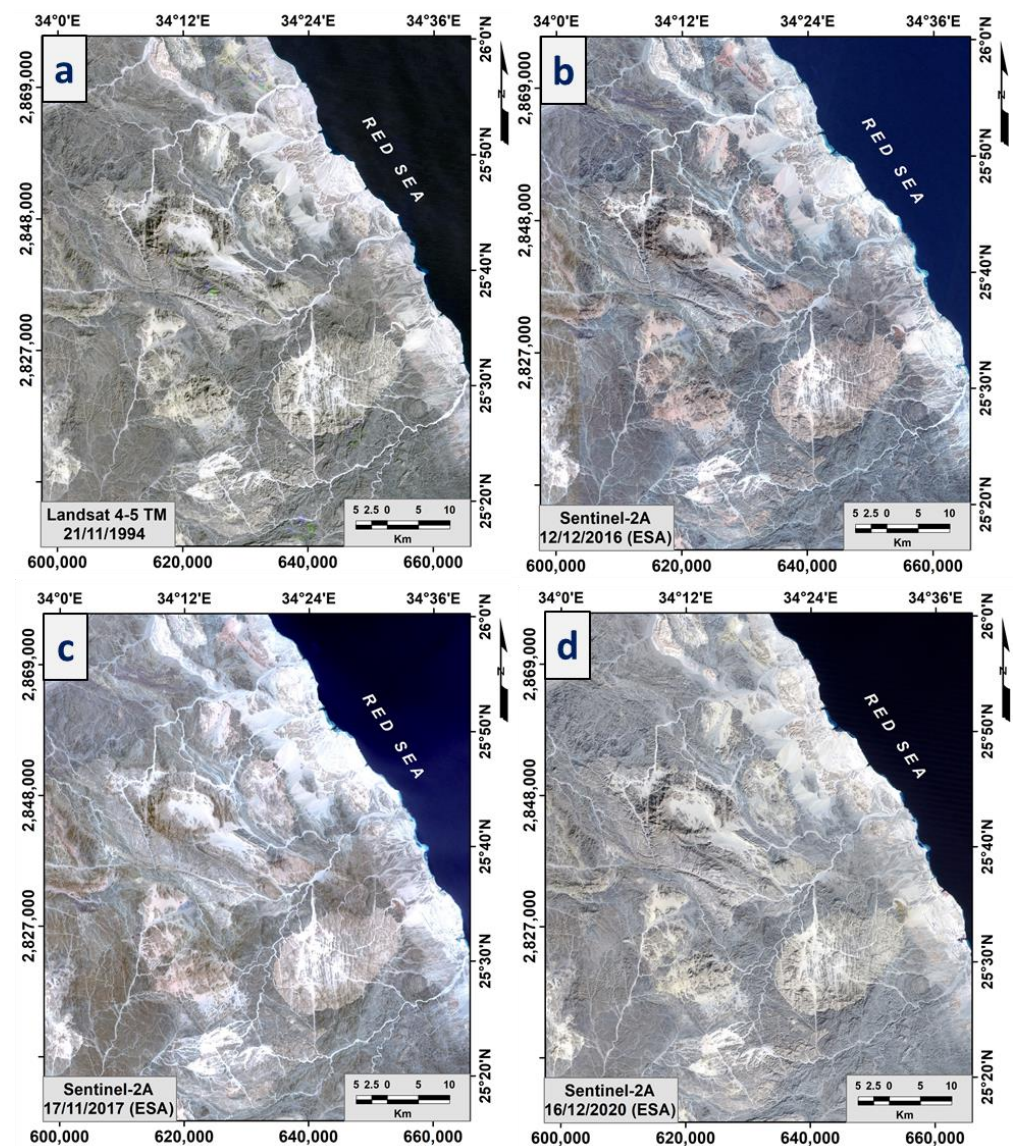


**Figure A2.** Landsat TM and sentinel-2A images of the study area in (a) 1994, (b) 2016, (c) 2017, and (d) 2000.

## References

1. Abdelmohsen, K.; Sultan, M.; Save, H.; Abotalib, A.Z.; Yan, E. What can the GRACE seasonal cycle tell us about lake-aquifer interactions? *Earth-Sci. Rev.* **2020**, *211*, 103392. [[CrossRef](#)]
2. Khalil, M.M.; Tokunaga, T.; Heggy, E.; Abotalib, A.Z. Groundwater mixing in shallow aquifers stressed by land cover/land use changes under hyper-arid conditions. *J. Hydrol.* **2021**, *598*, 126245. [[CrossRef](#)]
3. McCarthy, J.J.; Canziani, O.F.; Leary, N.A.; Dokken, D.J.; White, K.S. (Eds.) *Climate Change 2001: Impacts, Adaptation, and Vulnerability: Contribution of Working Group II to the Third Assessment Report of the Intergovernmental Panel on Climate Change*; Cambridge University Press: Cambridge, UK, 2001; Volume 2.
4. Abdel-Fattah, M.; Kantoush, S.; Suni, T. Integrated management of flash flood in wadi system of Egypt: Disaster prevention and water harvesting. *J. Annu. Disas. Prev. Res. Inst. Kyoto Univ.* **2015**, *58*, 485–496.
5. Prama, M.; Omran, A.; Schröder, D.; Abouelmagd, A. Vulnerability assessment of flash floods in Wadi Dahab Basin, Egypt. *Environ. Earth Sci.* **2020**, *79*, 114. [[CrossRef](#)]
6. Murray, V.; Ebi, K.L. IPCC special report on managing the risks of extreme events and disasters to advance climate change adaptation (SREX). *J. Epidemiol. Community Health* **2012**, *66*, 759–760. [[CrossRef](#)]
7. Attwa, M.; El Bastawesy, M.; Ragab, D.; Othman, A.; Assagaf, H.M.; Abotalib, A.Z. Toward an integrated and sustainable water resources management in structurally-controlled watersheds in desert environments using geophysical and remote sensing methods. *Sustainability* **2021**, *13*, 4004. [[CrossRef](#)]

8. Abotalib, A.Z.; Heggy, E.; El Bastawesy, M.; Ismail, E.; Gad, A.; Attwa, M. Groundwater mounding: A diagnostic feature for mapping aquifer connectivity in hyper-arid deserts. *Sci. Total Environ.* **2021**, *801*, 149760. [CrossRef]
9. Sultan, M.; Yan, E.; Sturchio, N.; Wagdy, A.; Gelil, K.A.; Becker, R.; Manocha, N.; Milewski, A. Natural discharge: A key to sustainable utilization of fossil groundwater. *J. Hydrol.* **2007**, *335*, 25–36. [CrossRef]
10. Yousif, M.; Henselowsky, F.; Bubenzer, O. Palaeohydrology and its impact on groundwater in arid environments: Gebel Duwi and its vicinities, Eastern Desert, Egypt. *Catena* **2018**, *171*, 29–43. [CrossRef]
11. Aljammaz, A.; Sultan, M.; Izadi, M.; Abotalib, A.Z.; Elhebiry, M.S.; Emil, M.K.; Abdelmohsen, K.; Saleh, M.; Becker, R. Land subsidence induced by rapid urbanization in arid environments: A remote sensing-based investigation. *Remote Sens.* **2021**, *13*, 1109. [CrossRef]
12. Pradhan, B. Flood susceptible mapping and risk area delineation using logistic regression, GIS and remote sensing. *J. Spat. Hydrol.* **2010**, *9*, 4.
13. Alshehri, F.; Abuamarah, B.A.; El-Hamid, H.T.A. Impact of land use dynamics on land surface temperature using optical remote sensing data integrated with statistical analysis in Riyadh, Saudi Arabia. *Adv. Space Res.* **2023**, *72*, 1739–1750. [CrossRef]
14. Abd El Aal, A.; Kamel, M.; Al-Homidy, A. Using remote sensing and GIS techniques in monitoring and mitigation of geohazards in Najran Region, Saudi Arabia. *Geotech. Geol. Eng.* **2019**, *37*, 3673–3700. [CrossRef]
15. Elsadek, W.M.; Ibrahim, M.G.; Mahmod, W.E.; Kanae, S. Developing an overall assessment map for flood hazard on large area watershed using multi-method approach: Case study of Wadi Qena watershed, Egypt. *Nat. Hazards* **2019**, *95*, 739–767. [CrossRef]
16. Nasir, M.J.; Iqbal, J.; Ahmad, W. Flash flood risk modeling of swat river sub-watershed: A comparative analysis of morphometric ranking approach and El-Shamy approach. *Arab. J. Geosci.* **2020**, *13*, 1082. [CrossRef]
17. El-Hamid, A.; Taha, H.; Alshehri, F. Integrated remote sensing data and machine learning for drought prediction in Eastern Saudi Arabia. *J. Coast. Conserv.* **2023**, *27*, 48. [CrossRef]
18. Mohamed, M.; Othman, A.; Abotalib, A.Z.; Majrashi, A. Urban heat island effects on megacities in desert environments using spatial network analysis and remote sensing data: A case study from western Saudi Arabia. *Remote Sens.* **2021**, *13*, 1941. [CrossRef]
19. Embabi, N.S. *Landscapes and Landforms of Egypt*; Springer: Berlin/Heidelberg, Germany, 2018.
20. EMA (Egyptian Meteorological Authority). *Normals for Meteorological Surface Station from (1981–2010)*; Egyptian Meteorological Authority: Cairo, Egypt, 2019.
21. Elnazer, A.A.; Salman, S.A.; Asmoay, A.S. Flash flood hazard affected Ras Gharib city, Red Sea, Egypt: A proposed flash flood channel. *Nat. Hazards* **2017**, *89*, 1389–1400. [CrossRef]
22. Megahed, H.A.; El Bastawesy, M.A. Hydrological problems of flash floods and the encroachment of wastewater affecting the urban areas in Greater Cairo, Egypt, using remote sensing and GIS techniques. *Bull. Natl. Res. Cent.* **2020**, *44*, 188. [CrossRef]
23. Youssef, A.M.; Pradhan, B.; Hassan, A.M. Flash flood risk estimation along the St. Katherine road, southern Sinai, Egypt using GIS based morphometry and satellite imagery. *Environ. Earth Sci.* **2011**, *62*, 611–623. [CrossRef]
24. Helmi, A.M.; Zohny, O. Flash flood risk assessment in Egypt. In *Flash Floods in Egypt*; Springer: Berlin/Heidelberg, Germany, 2020; pp. 253–312.
25. Conoco. *Geological Map of Egypt, Scale 1:500,000, 1987*; Egyptian General Petroleum Corporation-Conoco Coral: Cairo, Egypt, 1987.
26. ArcGIS. Mapping Products | GIS Software Products—Esri, Version 10.2. 2014. Available online: <https://www.esri.com/en-us/arcgis/products/index> (accessed on 15 July 2021).
27. WMS. Downloads | Aquaveo.Com, Version 11.1.1. Build Date: 7 November 2019. 2019. Available online: <https://www.aquaveo.com/downloads-wms?s=WMS&v=11.0> (accessed on 15 July 2022).
28. ESA SNAP. Sentinel Application Platform | Product the European Space Agency Earth, Version 9.0, Released on 29 June 2022. 2022. Available online: <https://step.esa.int/main/download/snap-download/> (accessed on 5 March 2023).
29. Google Earth Pro. Professional | Product Google, Version 7.3. Build Date: 29 December 2022. 2022. Available online: <https://google-earth-pro.en.uptodown.com/windows/download> (accessed on 15 January 2023).
30. EGSA. *Topographical Maps of Egypt, Scale 1:50,000, Finnish Egyptian Project*; Egyptian General Survey Authority (EGSA): Giza, Egypt, 1989.
31. Forkuor, G.; Maathuis, B. *Comparison of SRTM and ASTER Derived Digital Elevation Models over Two Regions in Ghana-Implications for Hydrological and Environmental Modeling*; INTECH Open Access Publisher: London, UK, 2012; pp. 219–240.
32. Patel, A.; Katiyar, S.K.; Prasad, V. Performances evaluation of different open source DEM using Differential Global Positioning System (DGPS). *Egypt. J. Remote Sens. Space Sci.* **2016**, *19*, 7–16. [CrossRef]
33. El Shamy, I.Z. Recent recharge and flash flooding opportunities in the Eastern Desert, Egypt. *Ann. Geol. Surv. Egypt* **1992**, *18*, 323–334.
34. Davis, J.C. *Statics and Data Analysis in Geology*; Wiley: New York, NY, USA, 1975.
35. Zuidam, R.V. *Aerial Photo-Interpretation in Terrain Analysis and Geomorphologic Mapping (No.C25102)*; Smits Publishers: The Hague, The Netherlands, 1986.
36. Horton, R.E. Erosional development of streams and their drainage basins; hydrophysical approach to quantitative morphology. *Geol. Soc. Am. Bull.* **1945**, *56*, 275–370. [CrossRef]

37. Strahler, A.N. Quantitative analysis of watershed geomorphology. *Eos Trans. Am. Geophys. Union* **1957**, *38*, 913–920.
38. Shreve, R.L. Infinite topologically random channel networks. *J. Geol.* **1967**, *75*, 178–186. [[CrossRef](#)]
39. Strahler, A.N. Hypsometric (area-altitude) analysis of erosional topography. *Geol. Soc. Am. Bull.* **1952**, *63*, 1117–1142. [[CrossRef](#)]
40. Strahler, A.N. Quantitative geomorphology of drainage basin and channel networks. In *Handbook of Applied Hydrology*; McGraw-Hill: New York, NY, USA, 1964; pp. 4–39.
41. Schumm, S.A. The evolution of drainage systems and slopes in badland at Perth Amboy, New Jersey. *Geol. Soc. Am. Bull.* **1956**, *67*, 597–646. [[CrossRef](#)]
42. Patton, P.C. Drainage Basin Morphometry and Floods. In *Flood Geomorphology*; John Wiley & Sons: New York, NY, USA, 1988; pp. 51–64.
43. Miller, V.C. *A Quantitative Geomorphic Study of Drainage Basin Characteristics in the Clinch Mountain Area, Virginia and Tennessee*; Columbia University: New York, NY, USA, 1953.
44. Alshehri, F.; Abdelrahman, K. Integrated approach for the investigation of groundwater quality using hydrochemical and geostatistical analyses in Wadi Fatimah, western Saudi Arabia. *Front. Earth Sci.* **2023**, *11*, 1166153. [[CrossRef](#)]
45. Smith, K.G. Standards for grading texture of erosional topography. *Am. J. Sci.* **1950**, *248*, 655–668. [[CrossRef](#)]
46. Yousif, M. Combination of remote sensing, GIS and palaeohydrologic remarks for promoting the exploitation of water resources in the Sahara: Cases from the Red Sea Coast, Egypt. *Environ. Earth Sci.* **2020**, *79*, 222. [[CrossRef](#)]
47. Abdelkader, M.M.; Al-Amoud, A.I.; El Alfy, M.; El-Feky, A.; Saber, M. Assessment of flash flood hazard based on morphometric aspects and rainfall-runoff modeling in Wadi Nisah, central Saudi Arabia. *Remote Sens. Appl. Soc. Environ.* **2021**, *23*, 100562. [[CrossRef](#)]
48. Gregory, K.J. Fluvial processes in British basins. In *Geomorphology—Present Problems and Future Prospects*; Embleton, C., Brunsdon, D., Jones, D.K.C., Eds.; OUP: New York, NY, USA, 1978; pp. 40–72.
49. Zuchiewicz, W. Morphotectonic phenomena in the polish flysch Carpathians: A case study of the Eastern Beskid Niski Mountains. *Quest. Geogr. Spec. Issue* **1989**, *2*, 155–167.
50. Chopra, R.; Dhiman, R.D.; Sharma, P.K. Morphometric analysis of sub-watersheds in Gurdaspur district, Punjab using remote sensing and GIS techniques. *J. Indian Soc. Remote Sens.* **2005**, *33*, 531–539. [[CrossRef](#)]
51. Abdalla, F.; El Shamy, I.; Bamousa, A.O.; Mansour, A.; Mohamed, A.; Tahaon, M. Flash floods and groundwater recharge potentials in arid land alluvial basins, southern Red Sea coast, Egypt. *Int. J. Geosci.* **2014**, *5*, 971–982. [[CrossRef](#)]
52. Horton, R.E. Drainage-basin characteristics. *Trans. Am. Geophys. Union* **1932**, *13*, 350–361.
53. Singh, S.; Singh, M.B. Morphometric analysis of Kanhar river basin. *Natl. Geogr. J. India* **1997**, *43*, 31–43.
54. Singh, P.; Gupta, A.; Singh, M. Hydrological inferences from watershed analysis for water resource management using remote sensing and GIS techniques. *Egypt. J. Remote Sens. Space Sci.* **2014**, *17*, 111–121. [[CrossRef](#)]
55. Abdelkareem, M. Targeting flash flood potential areas using remotely sensed data and GIS techniques. *Nat. Hazards* **2017**, *85*, 19–37. [[CrossRef](#)]
56. Eze, E.B.; Efiog, J. Morphometric parameters of the Calabar River basin: Implication for hydrologic processes. *J. Geogr. Geol.* **2010**, *2*, 18.
57. Abduladheem, A.; Elmewafey, M.; Beshr, A.F.; Elnaggar, A.A. Using GIS based morphometry estimation of flood hazard impacts on desert roads in South Sinai, Egypt. *Int. J. Sci. Eng. Res.* **2015**, *6*, 1593–1599.
58. Kadam, A.K.; Jaweed, T.H.; Kale, S.S.; Umrikar, B.N.; Sankhua, R.N. Identification of erosion-prone areas using modified morphometric prioritization method and sediment production rate: A remote sensing and GIS approach. *Geomatics. Nat. Hazards Risk* **2019**, *10*, 986–1006. [[CrossRef](#)]
59. Kumar, A.; Samuel, S.K.; Vyas, V. Morphometric analysis of six sub-watersheds in the central zone of Narmada River. *Arab. J. Geosci.* **2015**, *8*, 5685–5712. [[CrossRef](#)]
60. Rai, P.K.; Mohan, K.; Mishra, S.; Ahmad, A.; Mishra, V.N. A GIS-based approach in drainage morphometric analysis of Kanhar River Basin, India. *Appl. Water Sci.* **2017**, *7*, 217–232. [[CrossRef](#)]
61. Sujatha, E.R.; Selvakumar, R.; Rajasimman, U.A.B.; Victor, R.G. Morphometric analysis of sub-watershed in parts of Western Ghats, South India using ASTER DEM. *Geomat. Nat. Hazards Risk* **2015**, *6*, 326–341. [[CrossRef](#)]
62. Melton, M.A. *An Analysis of the Relations among Elements of Climate, Surface Properties, and Geomorphology*; Columbia University: New York, NY, USA, 1957.
63. El Bastawesy, M.; White, K.; Nasr, A. Integration of remote sensing and GIS for modelling flash floods in Wadi Hudain catchment, Egypt. *Hydrol. Process. Int. J.* **2009**, *23*, 1359–1368. [[CrossRef](#)]
64. Wheeler, H.S.; Ballard, B.W.; Jolley, T.J. An integrated model of arid zone water resources: Evaluation of rainfall-runoff simulation performance. *Sustain. Water Resour. Under Increasing Uncertain.* **1997**, *240*, 395–405.
65. Zhang, Y.; Huang, C.C.; Pang, J.; Zha, X.; Zhou, Y.; Yin, S.; Wang, J. Comparative study of the modern flood slackwater deposits in the upper reaches of Hanjiang and Weihe River Valleys, China. *Quat. Int.* **2012**, *282*, 184–191. [[CrossRef](#)]
66. Benito, G.; Thorndycraft, V.R. Palaeoflood hydrology and its role in applied hydrological sciences. *J. Hydrol.* **2005**, *313*, 3–15. [[CrossRef](#)]

67. Vittala, S.S.; Govindaiah, S.; Honne Gowda, H. Morphometric analysis of sub-watersheds in the Pavagada area of Tumkur district, South India using remote sensing and GIS techniques. *J. Indian Soc. Remote Sens.* **2004**, *32*, 351–362. [[CrossRef](#)]
68. Alshehri, F.; Sultan, M.; Karki, S.; Alwagdani, E.; Alsefry, S.; Alharbi, H.; Sahour, H.; Sturchio, N. Mapping the distribution of shallow groundwater occurrences using Remote Sensing-based statistical modeling over southwest Saudi Arabia. *Remote Sens.* **2020**, *12*, 1361. [[CrossRef](#)]

**Disclaimer/Publisher’s Note:** The statements, opinions and data contained in all publications are solely those of the individual author(s) and contributor(s) and not of MDPI and/or the editor(s). MDPI and/or the editor(s) disclaim responsibility for any injury to people or property resulting from any ideas, methods, instructions or products referred to in the content.